OCEANS & ATMOSPHERE FLAGSHIP
www.csiro.au

Remote sensing methods to map and monitor the condition of coastal habitats and other surrogates for biodiversity

Part B: Water quality mapping of the Van Diemen Gulf

Thomas Schroeder, Vittorio Brando, David Blondeau-Patissier, Lesley Clementson, Janet Anstee, Nandika Thapar and Edward King

Image Processing and Analysis Report

March 2015
Prepared for the NERP Northern Australia Hub

CHARLES DARWIN UNIVERSITY
National Environmental Research Program

Citation

Schroeder, T., Brando, V., Blondeau-Patissier, D., Clementson, L., Anstee, J., Thapar, N. and King, E. (2015), Remote Sensing Methods to map and monitor the condition of coastal habitats and other surrogates for biodiversity, Part B: Water quality mapping of the Van Diemen Gulf, Image Processing and Data Analysis Report, CSIRO Oceans & Atmosphere Flagship, Australia.

Copyright and disclaimer

Important disclaimer

Cover photographs

Left: MODIS-Aqua image covering the Van Diemen Gulf region (Courtesy NASA). Right: Instrumentation to measure water optical properties (Courtesy Michael Lawrence-Taylor).

Contents

Figures

Tables

1 Introduction

There is a paucity of biological data across the remote and inaccessible northern Australian coastline that currently constrains bioregional planning processes, development approvals and, ultimately, the conservation of biodiversity. Biophysical factors such as water depth, light availability and water quality are important determinants of coastal and marine biological communities and may be used as effective surrogates (Schroeder et al., 2012, Kennedy et al., 2012) in biodiversity assessments.

The natural resource management of the Van Diemen Gulf encompassing Kakadu National Park would benefit from long-term monitoring of key biophysical parameters where often little is known about biodiversity and ecosystem processes. Areas that are potentially transitional in the face of climate change or habitat refuge can be effectively identified and monitored from satellite observations. However, the optical complexity and large tidal range of the Van Diemen Gulf's coastal waters have limited the understanding of the region's water quality and its spatial and temporal variability. The remote location of this region also makes the acquisition of further knowledge of this particular marine system by conventional (ground-based) sampling methods difficult. However, recent developments in the area of physics-based water quality retrieval using satellite remote sensing allow more frequent and accurate large-scale water quality estimates from space than was previously possible. Remote sensing provides a cost-effective monitoring and trend assessment tool that can assist coastal zone management especially in remote and data-sparse regions such as the Van Diemen Gulf.

1.1 Project objectives

This report documents the adaptation and evaluation of a regional coastal water quality algorithm for the Van Diemen Gulf region with the main objective to provide an eleven year time series of key water quality parameters from daily observations of the Moderate Resolution Imaging Spectrometer (MODIS-Aqua) satellite. However, the application of this data to derive trends and to quantify change for specific regions that can be linked to other biodiversity assessments was out-of-scope of this project.

The production of MODIS data was performed at Australia's high-performance National Computational Infrastructure (NCI, http://nci.org.au) and utilized archiving and processing facilities developed and supported by the Integrated Marine Observing System (IMOS, http://www.imos.org). The retrieval of water quality from space is a multi-stage process with the project-specific workflow outlined in Figure 1. Daily MODIS Level 0 data acquisitions (e.g. raw counts) covering the study region were processed using NASA's SeaWiFS Data Analysis System (SeaDAS) software package version 7.0 (Fu et al., 1998). The most up-to-date calibration tables and other auxiliary inputs (e.g. meteorological information) were incorporated into the processing with SeaDAS to account for sensor degradation and to compute calibrated and geo-located radiances at Top-of-Atmosphere (TOA) as Level 2 outputs. A total number of 6,057 daily MODIS-Aqua files were processed from Level 0 to Level 2 quality using SeaDAS. These were subsequently re-projected from satellite swath geometry to an equal-rectangular grid (445 x 550 pixels) covering 130.5 °E to 133 °E in longitude and 11 °S to 13 °S in latitude (Figure 2). The re-projected data were further processed using CSIRO's Artificial Neural Network (ANN) atmospheric correction method (Schroeder et al., 2007) and its adaptive Linear Matrix Inversion (aLMI) in-water retrieval algorithm (Brando et al., 2012).

Parameterization of the aLMI for the Van Diemen Gulf region was achieved with ground observations collected during dedicated dry and wet season field voyages. The success of such an approach has largely been demonstrated in previous instances (Brando et al., 2012, Brando et al., 2014, Schroeder et al., 2012, King et al., 2014), however algorithm parameterization was not possible until recently because of the lack of in-situ measurements. The optical properties and concentrations presented in this report are the first to have been collected in the Van Diemen Gulf region. Ground observations were also used to evaluate the accuracy of remotely sensed water quality products, such as chlorophyll-a (CHL), total suspended solids (TSS) and coloured dissolved organic matter (CDOM).

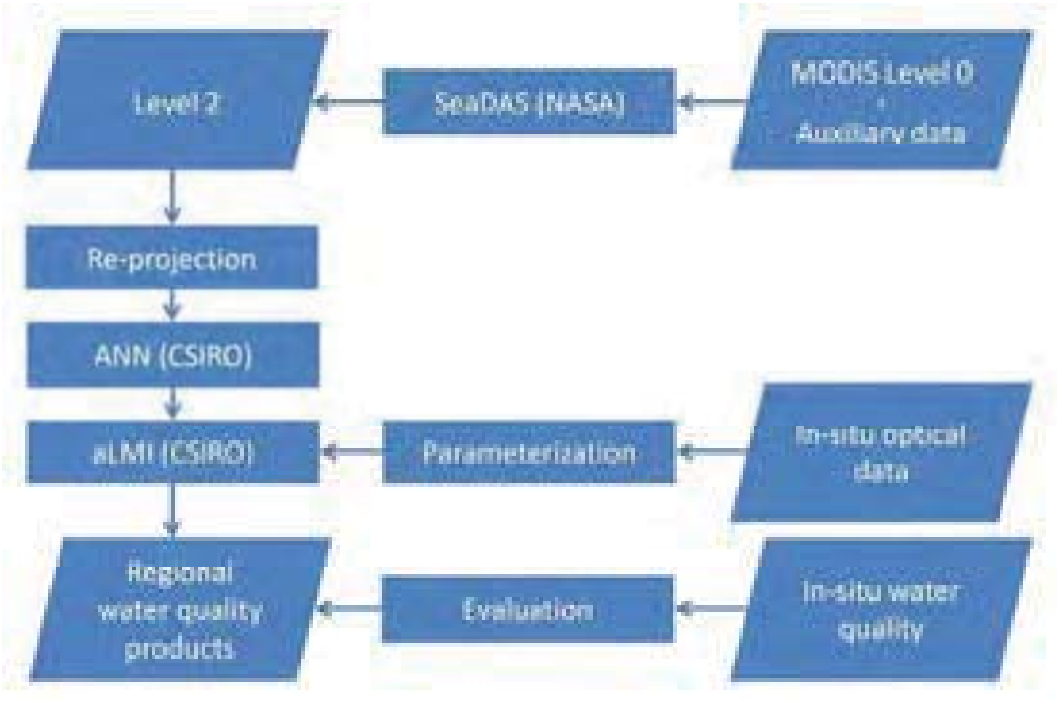

Figure 1 Satellite and in-situ data processing flow chart of this study

Specific project outputs are:

- A first bio-optical and biogeochemical characterization of the Van Diemen Gulf coastal waters capturing wet and dry season conditions.
- A validated time series of remotely sensed water quality for the Van Diemen Gulf covering 11+ years (July 2002 – September 2013).
- This report describing data acquisition, processing and analysis.

1.2 The regional environment of the Van Diemen Gulf

The Van Diemen Gulf is a semi-enclosed bay (~16,000 km^2) with two narrow passages (~25-30 km wide), one to the North into the Arafura Sea and a second to the West into the Beagle Gulf (Figure 2). It is a dynamic marine environment that is influenced by a tropical monsoonal climate, shallow depths (<20m) and strong tidal currents (mean spring tides range from 4 to 6 m). Five major river catchments surround the Van Diemen Gulf: the West, South (10,000 km^2) and East Alligator rivers on the East and the Mary (8,000 km^2) and the Adelaide rivers (638 km^2) on the west. While the western catchments have been actively used for agricultural purposes, mainly cattle grazing, the eastern catchments are mainly set aside for conservation (indigenous lands and national parks, such as the world heritage listed Kakadu National Park).

Monsoonal rainfall (~1,700 $mm \cdot yr^{-1}$)[1] generates large quantities of freshwater runoff that enter the coastal waters during the wet season via the surrounding catchments. The dry season spans from May to October, while the wet season extends from November to April, during which more than three-quarter of the annual rainfall occurs[1]. Cloud cover severely limits water quality remote sensing during the wet season months (see Figure 14). Monsoonal winds are mostly north-westerly, and vary in intensity, while south-easterly trade winds predominate during the dry season. These winds may significantly enhance resuspension of suspended sediments when acting in phase with tidally induced currents.

The Van Diemen Gulf remains largely understudied and literature on in-situ optical measurements linked to remote sensing of coastal water quality does not exist to our knowledge.

[1]BOM Bureau of Met., 73 year statistics (1941-1974) http://www.bom.gov.au , Climate statistics for Australian locations: Darwin Airport

2 In-situ optical observations

Due to the lack of bio-optical observations and their need for algorithm parameterization and evaluation, two comprehensive field voyages were accomplished in March 2012 and September 2013 capturing wet and dry season conditions. In total 58 sites (Figure 2) were sampled and profiled using a suite of commercial optical instruments to collect inherent and apparent optical properties in addition to biogeochemical concentrations.

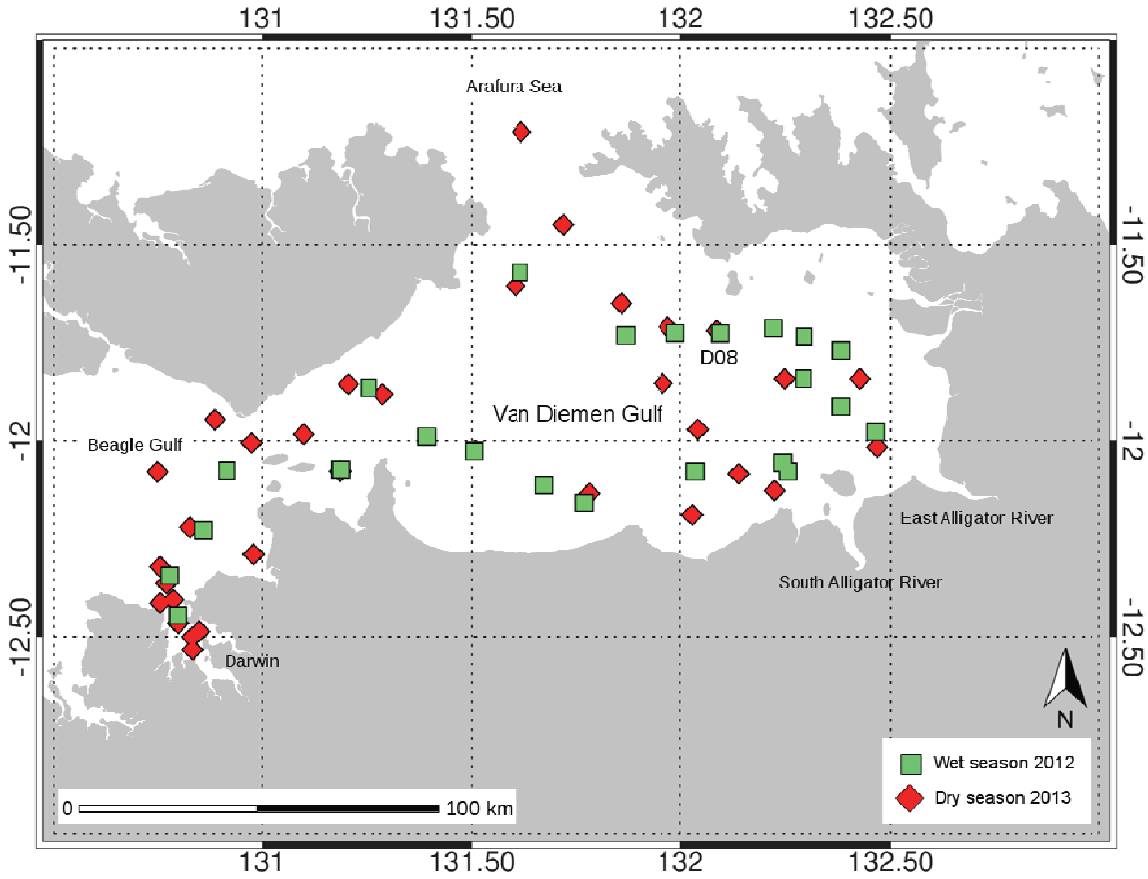

Figure 2 Location of measurement sites where optical and biogeochemical data was collected during the 2012 wet and 2013 dry season field voyages (N=58).

2.1 Inherent optical (IOP) measurements

At each site vertical profiles of the dissolved plus particulate absorption $a_{CDOM+p}(\lambda)$ and attenuation spectral coefficients c(λ) were measured using a 10-cm path length WET Labs (http://wetlabs.com) ac-s spectral absorption-attenuation meter. The total scattering coefficient b(λ) was computed from the difference between the attenuation and absorption coefficients of the ac-s. In addition, backscattering coefficients $b_b(\lambda)$ were measured using a WET Labs BB-9 spectral backscattering meter while temperature, salinity and density were collected using a WET Labs Water Quality Monitor. The backscattering measurements were corrected for salinity and light loss due to absorption over the path length using the absorption and scattering values from the ac-s (Boss et al., 2004). Profiles were measured with all instruments connected to a WET Labs DH-4 data logger allowing consistent time stamping. Further a freshwater Secchi disk was deployed at each site to visually estimate the water transparency. Specific inherent optical properties SIOPs were calculated subsequently by normalizing the IOP measurements to their respective biogeochemical concentrations.

2.2 Biogeochemical measurements

Surface water (≤2m) samples were collected concurrent to the IOP measurements following standard protocols for coastal waters (Tilstone et al., 2002) and were immediately filtered onboard and stored appropriately for further analysis in the laboratory at a later time. Total chlorophyll-a samples were filtered onboard through Whatman GF/F glass fibre filters (pore size ~0.7 µm) and stored in cryovial containers in liquid nitrogen. Coloured dissolved organic matter (CDOM) was filtered through a Whatman ANODISC filter (pore size 0.2 µm) and stored in glass bottles. Per 100 ml CDOM filtrate, 0.5 ml of a solution of sodium azide (10 g L^{-1}) was added to preserve the samples that were then stored in cool and dark conditions until analysis. Total suspended solids were filtered onto Whatman GF/F glass fibre filter (pore size 0.7 µm). In the laboratory phytoplankton pigments were analysed by High Performance Liquid Chromatography (HPLC) using the method of Clementson (2013) and concentrations of total suspended solids were determined by gravimetric analysis. In addition, algal, non-algal and coloured dissolved organic (CDOM) absorption was measured, using a dual beam UV/VIS spectrophotometer fitted with an integrating sphere. The spectral slope of CDOM was computed by non-linear regression to fit the absorption coefficients between 400 and 700 nm. A more detailed description of the methods for all these measurements can be found in Oubelkheir et. al (2014).

2.3 Apparent optical (AOP) measurements

Light attenuation profiles were measured at each station using a Satlantic free-falling optical profiler (http://satlantic.com). Subsequently the profiler was deployed with a flotation collar to acquire measurements of the upwelling radiance field just below the water surface and the down-welling irradiance above water. An additional down-welling irradiance sensor was mounted up high on the vessel which provided a more stable platform. The radiance and irradiance data was quality controlled by filtering for sensor tilts less than 5 degrees and converted into above-water reflectance. The reflectance data was used to assess the suitability of the IOP data for algorithm parameterization by quantifying optical closure as described in section (4.3.2).

2.4 Summary data overview

Table 1 Range of quality controlled optical and biogeochemical measurements collected during the field voyages.

	Dry season (2013)					Wet season (2012)				
Variable	N	Min	Max	Mean	Std Dev	N	Min	Max	Mean	Std Dev
CHL [mg m^{-3}]	29	0.33	2.79	0.86	0.45	11	0.33	1.61	0.85	0.37
TSS [g m^{-3}]	29	2.69	482.77	56.52	87.54	14	1.74	8.33	4.28	1.84
a_{CDOM} 440 [m^{-1}]	28	0.05	0.70	0.16	0.13	14	0.08	0.85	0.28	0.25
S_{CDOM} [m^{-1}]	28	0.005	0.017	0.013	0.003	14	0.009	0.017	0.014	0.001
a_{PHY} (440) [m^{-1}]	29	0.023	1.077	0.104	0.204	11	0.033	0.088	0.052	0.018
a_{PHY}* (440) [m^2 mg^{-1}]	29	0.034	0.386	0.090	0.077	11	0.025	0.125	0.069	0.031
a_{NAP} (440) [m^{-1}]	29	0.045	5.420	0.498	1.088	11	0.026	0.198	0.077	0.051
S_{NAP} [m^{-1}]	29	0.011	0.019	0.014	0.002	11	0.012	0.015	0.014	0.001
b_b (555)	22	0.031	0.736	0.194	0.263	12	0.014	0.323	0.065	0.085
Y_{NAP}	22	0.233	1.731	0.633	0.409	12	0.442	0.931	0.695	0.153
Temperature [°C]	23	26.3	28.7	27.6	0.7	11	29.5	31.2	30.1	0.5
Salinity	23	34.3	35.1	34.6	0.3	11	19.0	32.8	28.9	4.4
Secchi [m]	29	0.3	4.0	2.1	1.1	14	1.5	5.5	2.8	1.0

3 Remote sensing observations

3.1 The MODIS-Aqua sensor

The MODIS imaging radiometer has been operational since May 2002 on board of NASA's Earth Observing System (EOS) Aqua polar-orbiting spacecraft. Its high sensitivity and large dynamic range enables MODIS to accurately monitor the Earth's atmosphere and surface. With the spacecraft orbiting sun-synchronous at an altitude of 705 km, MODIS measures the reflected solar and thermal radiation in 36 spectral bands ranging in wavelength from 0.14 µm to 14.5 µm, with a spatial resolution of 250 m (2 bands), 500 m (5 bands) and 1000 m (29 bands) at nadir. The instrument view's the Earth's surface over a ±55 field-of-view (FOV) range relative to the instrument nadir across-track flight direction using a two-sided scan mirror that rotates at 20.3 r min^{-1} (Xiong and Barnes, 2006). Each scan covers an across-track swath of 2.330 km and Aqua's celestial orbit allows MODIS to cover the Earth's surface completely in 1-2 days, depending on latitude. High spectral, spatial and temporal resolution makes the MODIS instrument ideal for environmental monitoring.

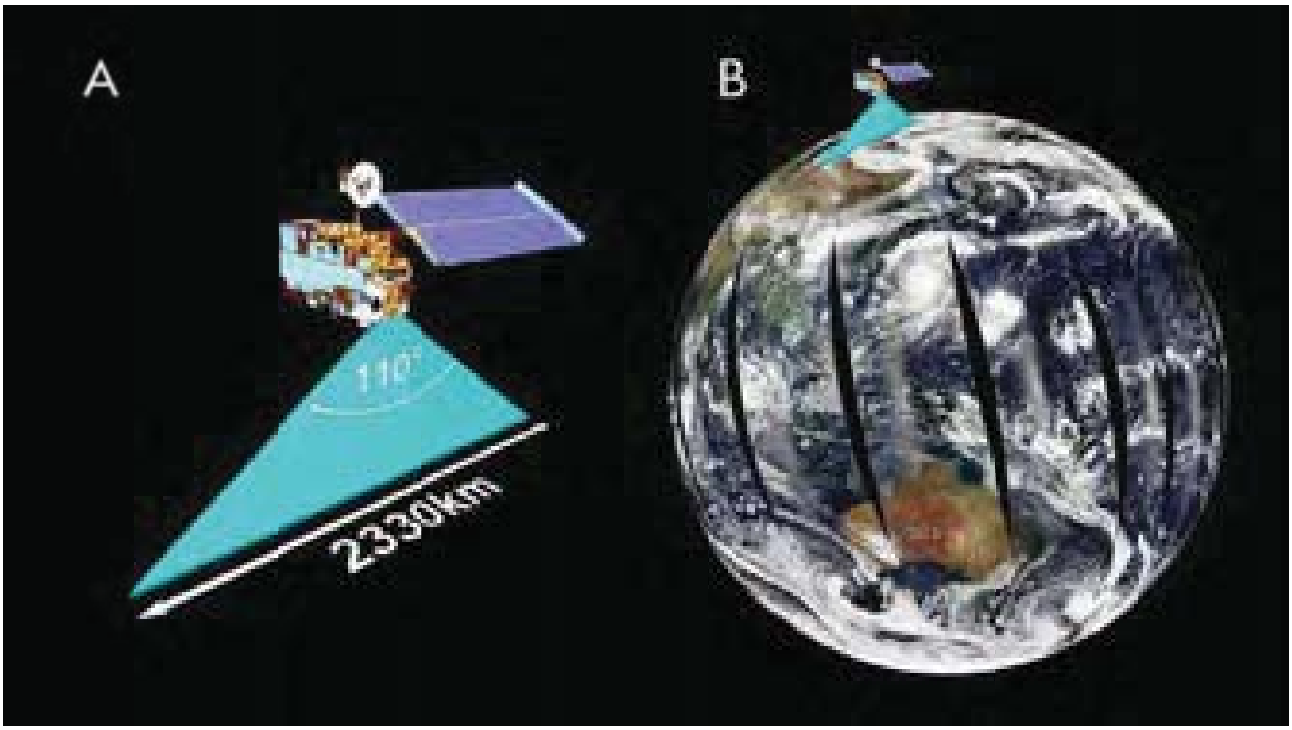

Figure 3 Swath illustration of MODIS (A) and polar-orbiting principle of the satellite scanning the upward reflected solar irradiance of the Earth's surface from which geophysical products can be derived (B). Image credits: NOAA.

Figure 4 presents two example MODIS-Aqua true colour images that illustrate the optical complexity and contrasting seasonal differences of the Van Diemen Gulf coastal waters during or close to the 2012/2013 field voyages. Nearly at the end of the wet season, large amounts of river run-off still discharge into the Van Diemen Gulf and mix with the coastal waters (Figure 4a). Dissolved organic matter and phytoplankton that absorb light in the blue spectral region discolour the near-shore waters dark greenish. Creeks discharge small distinct plumes of brownish TSS and CDOM dominated waters into the Gulf, while a large greenish patch, probably TSS and phytoplankton-rich waters flush into the Arafura Sea and get diverted to the west following the main current. In the absence of any terrestrial inputs from river run-off during the dry season the system is entirely dominated by tidal resuspension of TSS (Figure 4b).

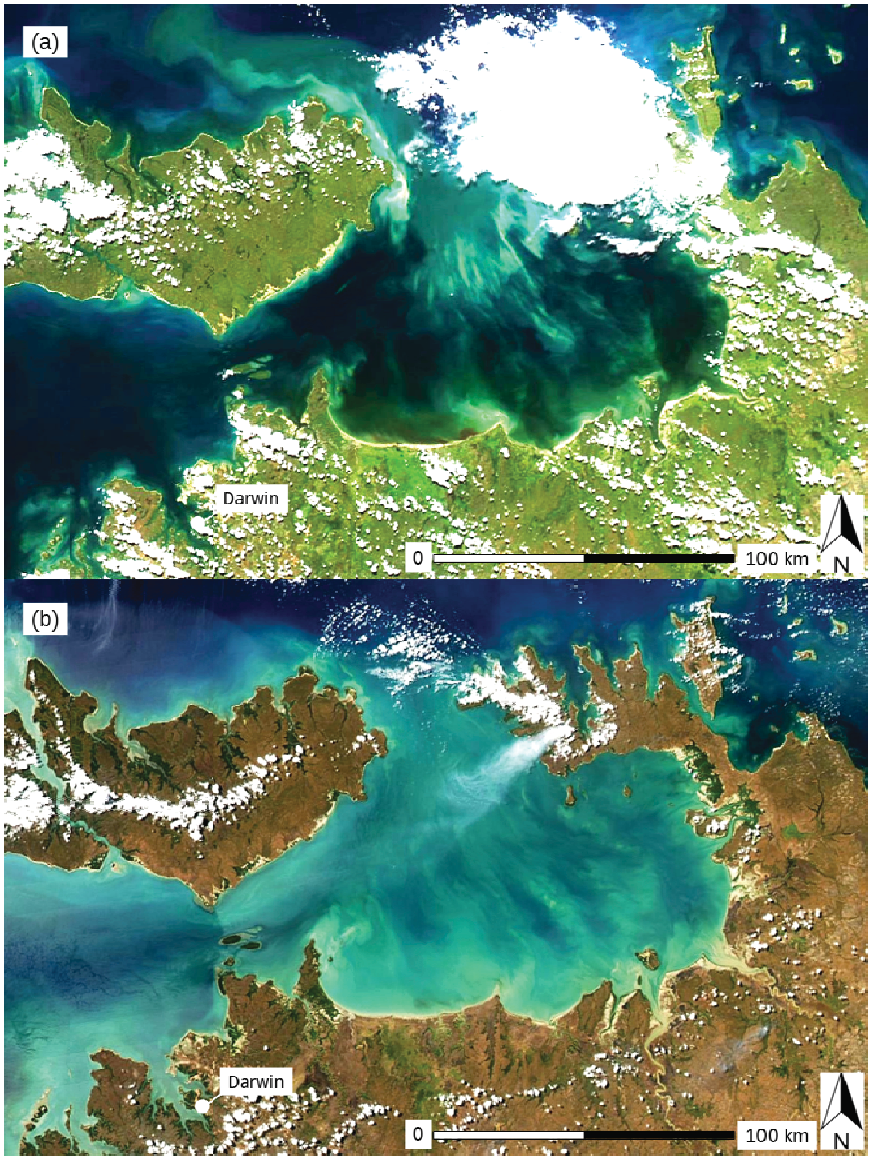

Figure 4 MODIS-Aqua true-colour images covering the Van Diemen Gulf and Darwin Harbor regions on (a) 2 April 2012 (wet season) and (b) 14 Sep 2013 (dry season) illustrating the optical complexity and contrasting seasonal differences in water colour.

3.2 Atmospheric correction

Accurate atmospheric correction is a prerequisite for quantitative ocean colour remote sensing and remains a challenge above optically complex coastal waters, such as the Van Diemen Gulf, due to the difficulty of separating atmospheric and oceanic signals (IOCCG, 2010). Atmospheric correction is the process of removing the effects of Rayleigh and Mie scattering as well as absorption of atmospheric gases and certain types of aerosols from remotely sensed imagery. Over the ocean atmospheric scattering contributes up to 90% to the remotely sensed signal at the top-of atmosphere. Removing the variable atmospheric bias is required to enable multi-temporal image analysis. Only the water-leaving radiance or reflectance (at the sea surface) contains spectral information about optically significant water constituents such as chlorophyll-a, CDOM and TSS.

The atmospheric correction approach implemented for this study is based on inverse modelling of radiative transfer simulations in a coupled ocean-atmosphere system using artificial neural networks (Schroeder et al., 2007). The algorithm is well suited for coastal waters and detailed validation results are published in Goyens et al. (2013) and King et al. (2014). Atmospheric correction outputs are used as input to the in-water retrieval algorithm (Figure 1). The theoretical basis and regional parameterization of the in-water retrieval algorithm using the field observations (see section 2) are described in detail in the next section.

4 Inverse in-water algorithm parameterization

4.1 Algorithm approach to address optical complexity and seasonal variability

The goal of the satellite data processing system is to retrieve the inherent optical properties (IOPs) of the water, and relate them to the physical constituents, by analysis of the atmospherically corrected reflectance spectra at the water surface.

As shown in Section 2, the field activities demonstrated a large variability in optical properties of the dissolved and particulate matter in the Van Diemen Gulf between the dry and wet seasons (see Table 1). In this study the approach previously developed by CSIRO to accurately derive water quality in the Great Barrier Reef (GBR) lagoon waters has been adopted and parameterised for the optical conditions of Van Diemen Gulf.

4.2 Context - Algorithm approach for the Great Barrier Reef

To improve the accuracy of water quality retrievals from MODIS-Aqua data in GBR Lagoon coastal waters, CSIRO developed an adaptive approach that extends a linear matrix inversion technique developed by Hoge and Lyon (1996). The adaptive linear matrix inversion (aLMI) technique simultaneously estimates the IOPs and concentrations of CHL, non-algal particulate matter (NAP) and CDOM from atmospherically corrected spectra (Brando et al. 2012, King et al. 2014).

This adaptive implementation of the LMI was specifically developed to incorporate regional and seasonal knowledge of variability in the specific inherent optical properties for concentration, specific light absorption and scattering encountered in GBR coastal waters (Brando et al., 2008; Brando et al., 2014; Brando et al., 2012). The aLMI method uses the below-water remote sensing reflectance spectrum $r_{rs}(\lambda)$ of MODIS bands 8-15 (412-748 nm) as input to a semi-analytical model developed by Gordon et al. (1988) to simultaneously derive the three optically active constituents in an algebraic manner. One of the major weaknesses of the LMI is the difficulty of parameterising a stable spectral shape for each SIOP to reflect the natural variability (Lyon and Hoge 2006). In aLMI, to incorporate regional knowledge of specific IOPs, the inversion of imagery is performed while varying the SIOP shape factors through a small group of predetermined combinations, i.e. the candidate model parameter sets (Brando et al., 2012). Each candidate model parameter set corresponds to a naturally occurring set of SIOP shape and amplitude factors ($a^*_{PHY}(\lambda)$, S_{CDOM}, $a^*_{NAP}(440)$, S_{NAP}, $b_b{}^*_{PHY}(555)$, and Y_{PHY} , $b_b{}^*_{NAP}(555)$ and Y_{NAP} see Table 1 of Brando et al. 2012 for precise definitions) estimated from a suite of in-situ measurements and samples collected concurrently at a sampling station during a field campaign, hence each of these model parameter sets is time, location and water-type specific. By performing the spectral inversion only for a limited number (L, Figure 5) of naturally occurring model parameter sets, unnatural (or highly unlikely) combinations of the SIOP shape and amplitude factors are avoided (Brando et al., 2012).

In aLMI the model parameter set, the IOPs and concentration values associated with the best optical closure $\Delta(r_{rs}$ input - r_{rs} model) are retained as the optimal solution for each inverted spectrum (Figure 5). With this approach, no *a priori* assumptions are made on the occurrence of a specific water mass at any given location during the inversion of satellite imagery. A more detailed description of the algorithm, together with complete definition of symbols, is provided in Brando et al. (2012). A description of the pre-operational implementation of the algorithm for monitoring GBR water quality is provided in King et al. (2014).

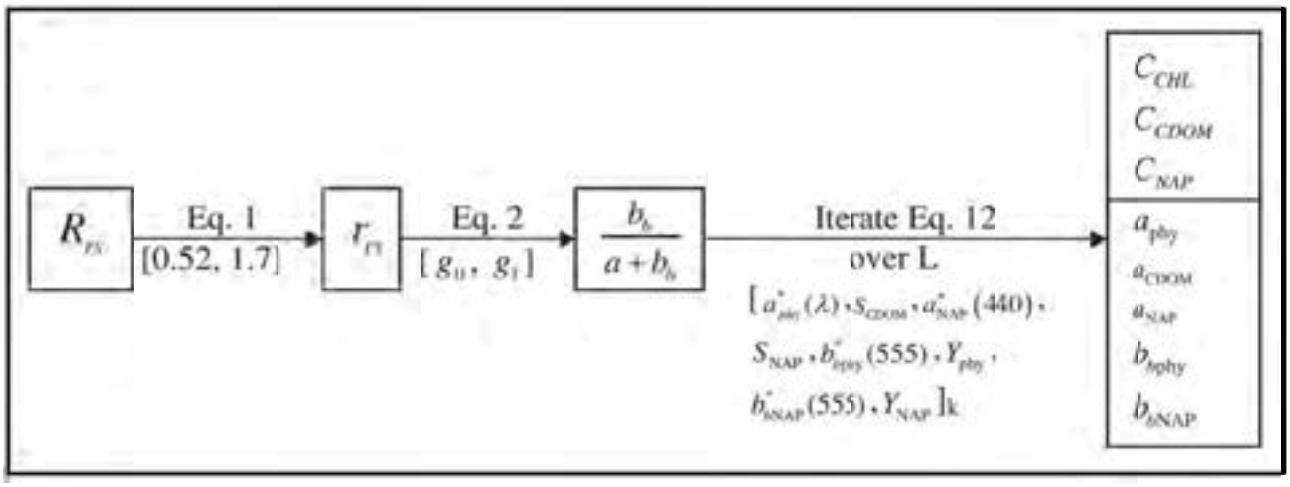

Figure 5 Conceptual diagram of the adaptive Linear Matrix Inversion approach adopted for the retrieval of concentrations and IOPs in the Van Diemen Gulf from MODIS-Aqua data (reproduced from Brando et al. 2012).

4.3 Extension of the algorithm approach to the Van Diemen Gulf

To adapt the aLMI approach to Van Diemen Gulf waters, Ocean Colour Radiometry (OCR) was simulated at MODIS bands for this optically complex system using the water properties measured during the dry and wet season field campaigns. The uncertainty associated with several parameterizations was evaluated following the sensitivity analysis methodology carried out in Brando et al. (2012).

To this aim, from the data acquired during the two fieldworks, only stations where all the SIOPs amplitude and shape factors were available were selected. The selected data is summarized in Figure 6. It is important to note that the SIOP parameters of the particulate matter show the most difference across the two seasons ($a^*_{NAP}(440)$, S_{NAP}, $b_b{}^*_{NAP}(555)$ and Y_{NAP}). Both SIOPs shape factors (S_{CDOM} and S_{NAP}) show different mean values across the seasons, and there was a marked difference between the SIOPs amplitude factors ($a^*_{NAP}(440)$ and $b_b{}^*_{NAP}(555)$) in the two seasons, where the values in the dry season are almost an order of magnitude higher than in the wet season. The difference in the SIOPs amplitude factors is mainly due from differences in TSS concentrations in the two seasons, as the ranges of the IOP amplitude factors ($a_{NAP}(440)$ and $b_{bNAP}(555)$) were similar. This is likely due to different processes controlling the particulate matter concentration and composition in the two seasons.

4.3.1 SIMULATED DATA SET

A MODIS reflectance dataset was simulated using radiative transfer modelling for Van Diemen Gulf based on measurements of SIOPs and concentrations. The concentrations of the three optically-active constituents (C_{CHL}, C_{NAP} and C_{CDOM}) as well as the SIOP parameters were varied to represent the bio-optical variability of the study site, similar to the simulated reflectance dataset used in Brando et al. (2012):

- A total of 594 simulations representing this case study region were conducted to generate IOPs, R_{rs}, r_{rs}, and u values for the MODIS spectral range.
- For each complete SIOP parameter set, 27 simulations were performed by varying C_{CHL}, C_{CDOM}, and C_{NAP} by -10%, 0% and +10% of the concentrations measured in situ.
- A four-component model was parameterized in Ecolight 5.1.4 with the 22 complete sets of SIOP shape and amplitude factors estimated from concurrent in situ measurements and samples collected during the two measurement campaigns.
- For the particles scattering phase function, the Fournier-Forand phase function with the backscattering ratio ($b_b(550)/b(550)$) estimated from in-situ measurements was selected for each complete SIOP parameter set (Figure 6).

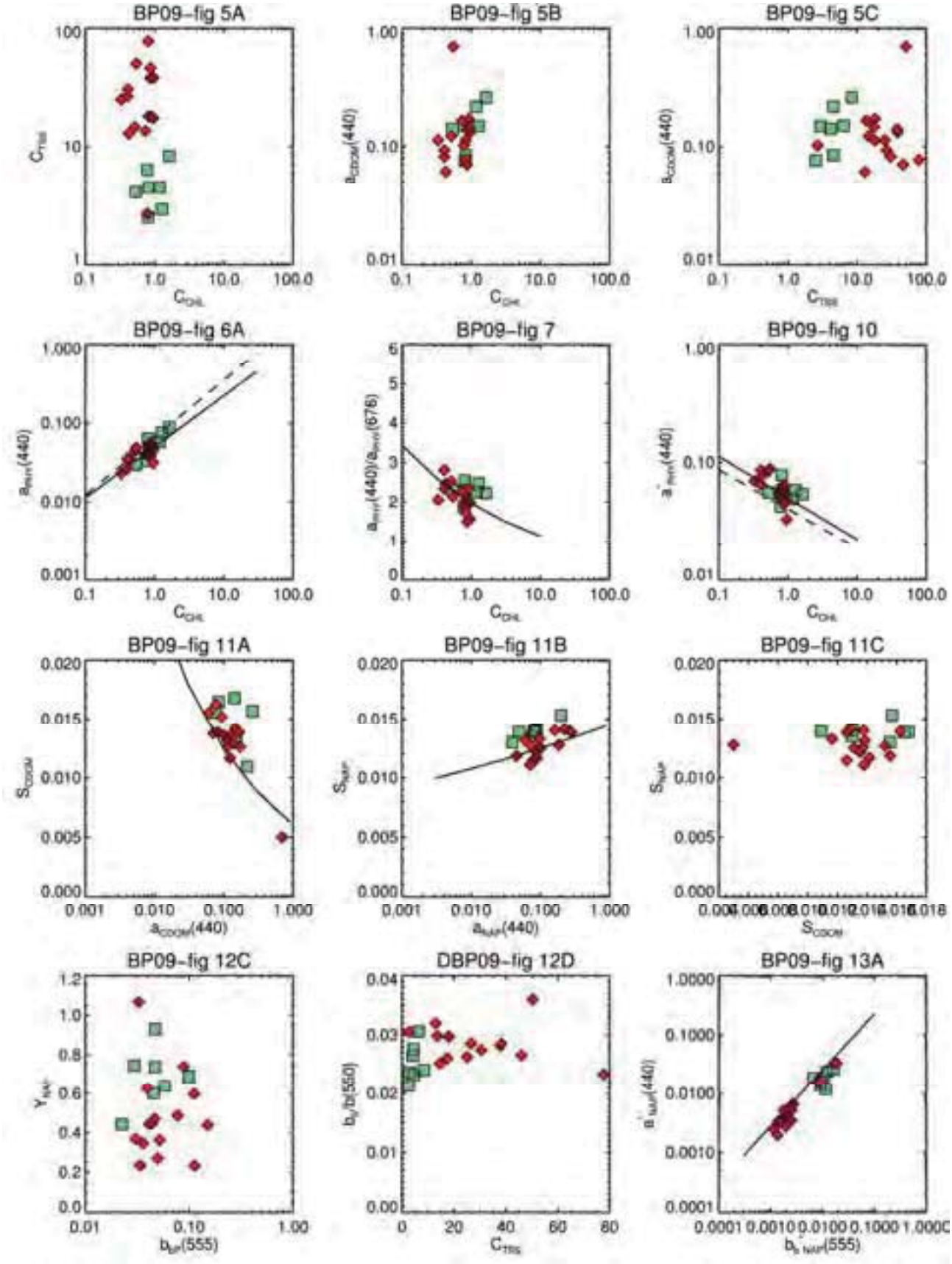

Figure 6 Summary of optical complexity for the Van Diemen Gulf waters, SIOP parameters for the stations used in the algorithm development. The twelve panels reproduce figures from Blondeau-Patissier et al. (2009); green boxes and red diamonds represent stations acquired during the wet and dry season respectively.

4.3.2 OPTICAL CLOSURE

In the literature, one approach to assess the uncertainty associated with the SIOP amplitude and shape factors is to evaluate the optical closure between modelled and measured R_{rs} spectra (e.g. Brando & Dekker 2003, Giardino et al., 2007, Chang et al., 2003). Figure 7 presents an example of this analysis for selected sites of the Van Diemen Gulf. Measured IOPs were used in a radiative transfer model to simulate the corresponding above water reflectance at each site, which were then compared against in-situ observed reflectance as reference data. Whilst for most stations a good match in terms of shape and intensity could be achieved, larger deviations occurred at VDGD8 and VDGD10 where the shape was found to be very similar but the intensities did not match. This may be attributed to uncertainties associated with the IOPs and concentrations used to estimate the SIOPs shape and amplitude factors, which were the inputs for the radiative transfer modelling, but also to those associated with the radiometric (AOP) measurements. In dynamic and optically complex systems such as Van Diemen Gulf short term variability due to strong tidal currents may explain differences between modelled and observed radiometry, especially for those sites where larger time differences between IOP and AOP measurements occurred (up to 30 minutes difference). However, it remains difficult to attribute the lack of optical closure to one of the data sources. The limited number of data points available for this modelling activity was also considered, hence all data was used for further analysis.

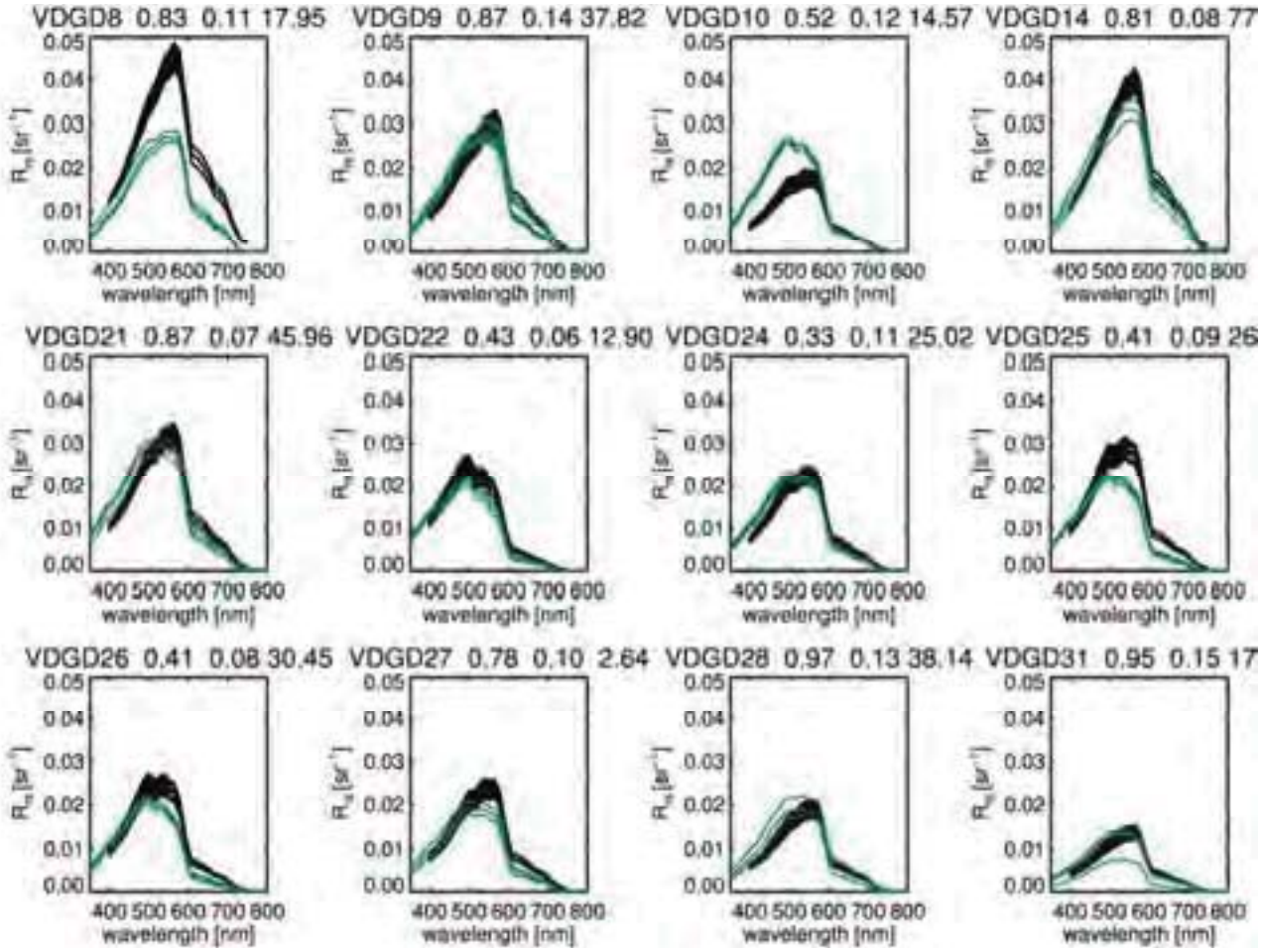

Figure 7 Optical closure between the simulated and measured above water remote sensing reflectance (Rrs) for 12 stations sampled during the 2013 dry season fieldwork. The black lines represent the 27 Hydrolight simulations performed for each station; the three blue lines present the range of measured spectra (minimum, median and maximum).

4.3.3 ALMI PARAMETRIZATION ADDRESSING SEASONAL VARIABILITY

Based on the seasonal variability in optical properties from the field data (Figure 6), four adaptive parameterizations for aLMI were defined, i.e. four groups of predetermined candidate model parameter sets were selected. Two adaptive parameterizations were derived by using the complete sets of SIOP shape and amplitude factors in each of the two seasons (VDG_D and VDG_W for the dry and wet season, respectively). The third adaptive parameterization was composed of all 22 complete sets of SIOP shape and amplitude factors from the two field campaigns (VDG_{DW}). A fourth adaptive "seasonal" parameterization (VDG_S) was devised by running the inversion of dry season spectra with dry season parameters while the wet season spectra were inverted with wet season parameters.

4.3.4 SENSITIVITY ANALYSIS OF ALMI PARAMETRIZATION

To assess the performance of the aLMI in VDG waters, the aLMI spectral inversion was applied to the simulated MODIS reflectance dataset by using the four model parameter sets defined above representing measurements performed in different seasons in this coastal system. Furthermore, to assess the uncertainties specifically introduced by the aLMI procedures and to set a benchmark for the aLMI inversions for the four parameterizations, the inversion for each R_{rs} spectrum of the simulated reflectance dataset was parameterized with the SIOP shape and amplitude parameters used in the forward simulation (OWN). Figure 8 presents the comparison between retrieved and input bulk IOPs for all four parameterizations (VDG_D, VDG_w, VDG_{DW} and VDG_S), while Figure 9 presents the comparison between retrieved and input concentrations. To summarize the accuracy of the retrieval of the four adaptive paramerizations Figure 10 presents the Taylor diagrams of bulk and apportioned IOPs, as well as concentrations. The Taylor diagrams represent three different statistics simultaneously: the normalized standard deviation, as the along-axis of the polar coordinate plot, the correlation coefficient, as the angular position, and the unbiased Root-Mean- Square Difference (RMSD), as the distance between the model point and the reference comparison point (Taylor, 2001, Jolliff et. al 2009).

Consistent with the findings of Brando et al. (2012), the benchmark parameterization provides very accurate retrieval of the bulk IOPs (R^2>99%, Figure 8, Figure 10) as well as the concentrations of C_{NAP} (R^2>99%, Figure 9, Figure 10), while C_{CHL} proves difficult to retrieve in the optically complex VDG waters (R^2=62%), as phytoplankton contributes only ~5-20% to the absorption budget (Brando et al 2012, Lee et al 2010).

For the VDG four parameterizations, the retrieval of a_{CDOM+P} and b_{bP} is very accurate (a_{CDOM+P}:R^2>96-98%; b_{bP}: R^2>99%), even while the total absorption shows some deviations from the 1:1 line, particularly for VDG_D and VDG_w. For the retrieval of the concentrations, large deviations from the 1:1 line were observed (C_{CHL}: R^2=1-49%; C_{CDOM}: R^2=18-96%; C_{NAP}: R^2=6-46%;). The accurate retrieval of C_{CDOM} for VDG_D, VDG_{DW} and VDG_S reflects the ability of aLMI to accurately apportion the total absorption to the optically active constituents (OACs) for these parameterizations, while the lower accuracy for $C_{CHL}$and C_{NAP} is due to the erroneous selection of the SIOP amplitude parameters relating concentrations and apportioned IOPs during the aLMI inversion process.

Figure 11 and Figure 12 present the histograms of the relative errors in the retrieval of the selected SIOP shape and amplitude parameters for the four aLMI parameterizations. It is important to note that due to the strong seasonal differences in the processes controlling the IOPs, the two single season parameterizations (VDG_D and VDG_W) miss some of the amplitude and shape factors used in the whole simulated set (Figure 6). Thus the distribution of the parameters selected during aLMI inversion process shows some gaps. This is particularly evident for the four shape parameters ($a^*_{PHY}(440)/a^*_{PHY}(676)$, S_{CDOM}, S_{NAP}, and Y_{NAP}) in VDG_W (Figure 11) and the NAP amplitude parameters (a^*_{NAP}, $b_b{}^*_{NAP}$, $b_{bP}(555)/b_P(555)$) for VDG_D and VDG_W (Figure 12). This explains the inaccurate apportioning of the bulk IOPs to the OACs observed for VDG_W (Figure 9, Figure 10) and the inaccurate retrieval of C_{CHL} and C_{NAP} for VDG_D and VDG_W (Figure 9, Figure 10). The "complete" and the "seasonal" parameterizations (VDG_{DW} and VDG_S) show a good distribution of the shape and amplitude parameters (Figure 11 and Figure 12), with the "seasonal" parameterization VDG_S selecting more often the whole SIOP shape and amplitude parameter sets used in the forward simulation (N=245).

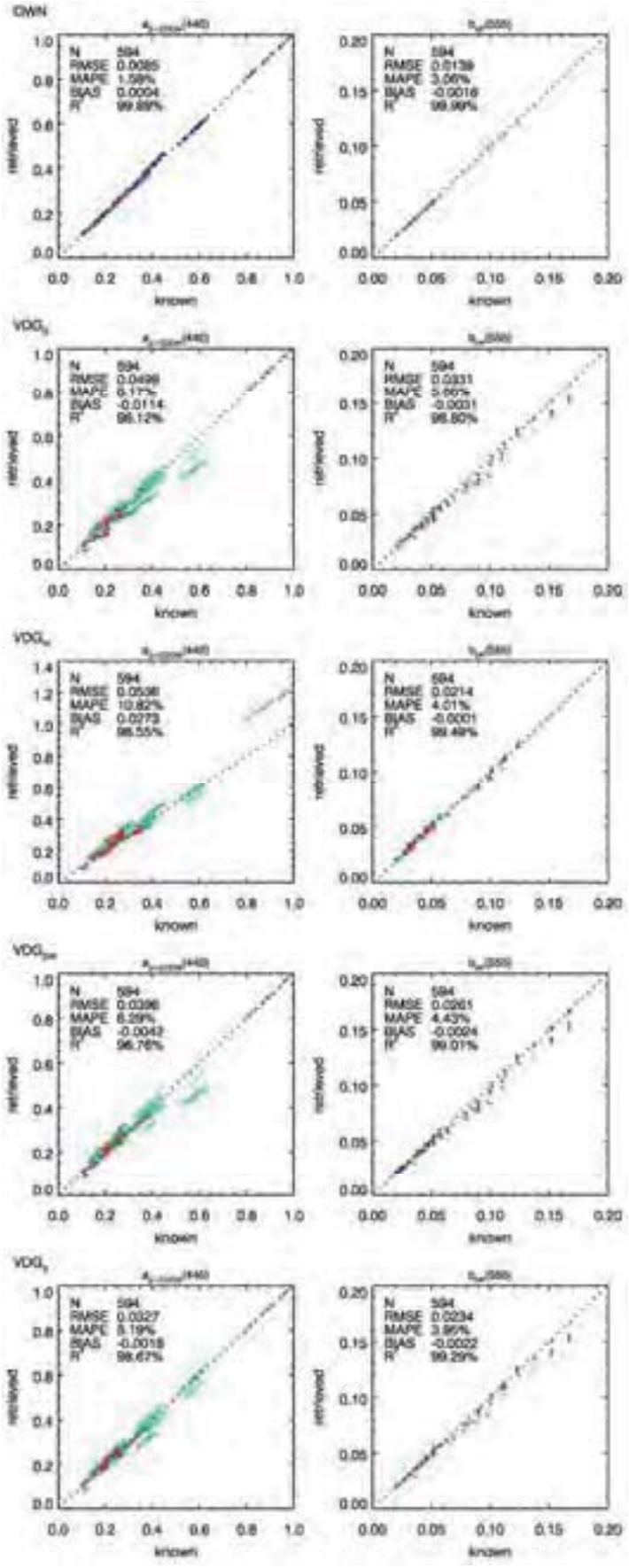

Figure 8 Comparison between retrieved and simulated bulk IOPs. The figure is organized in five rows (the model parameter sets), and in two columns (a and b_b). The scatterplot colors indicate density of points from blue (low density) to dark red (high density), the dotted line is the 1:1 line.

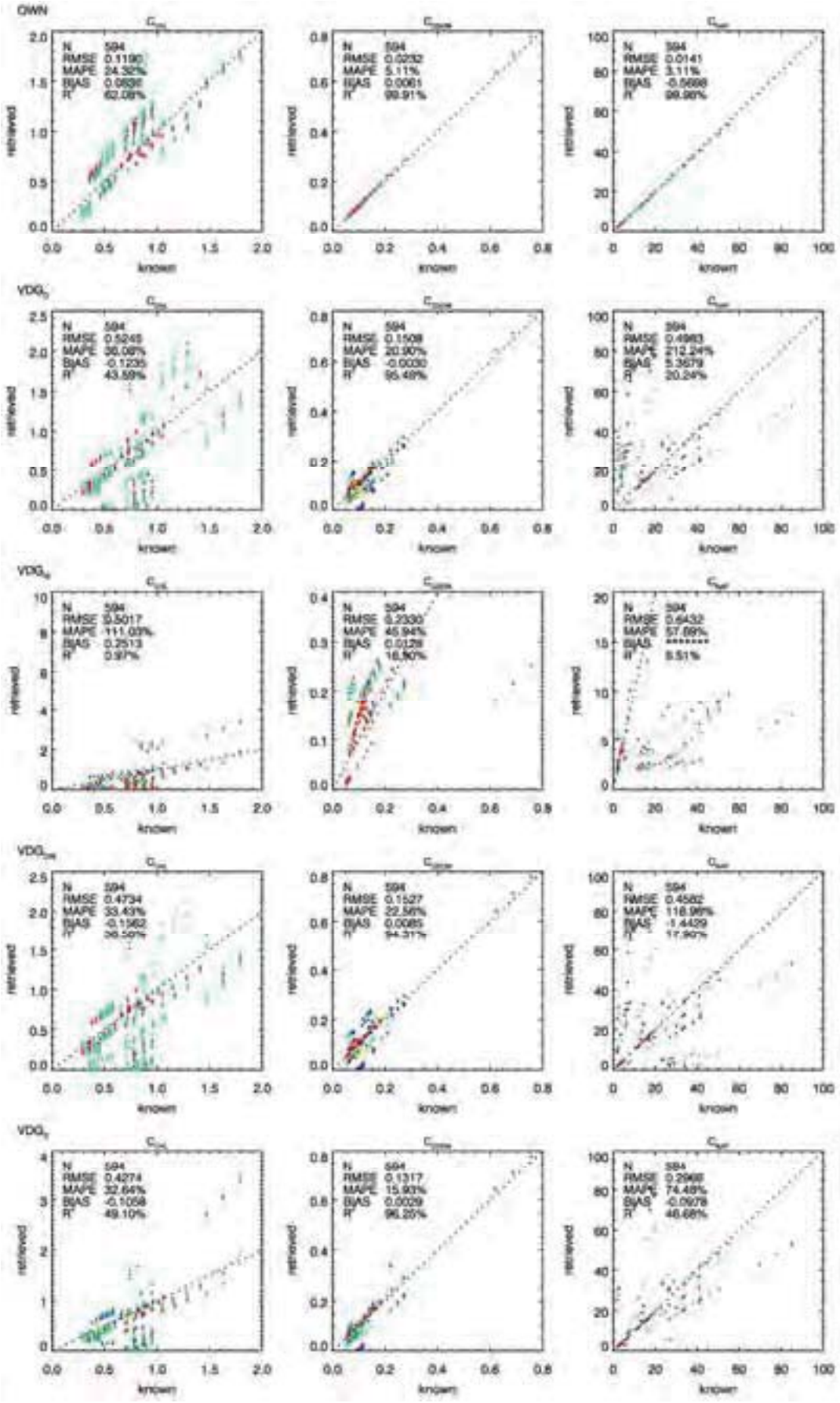

Figure 9 Comparison between retrieved and simulated concentrations. The figure is organized in five rows (the model parameter sets) and three columns (C_{CHL}, C_{CDOM}, and C_{NAP}). In the scatterplot colors indicate density of points from blue (low density) to dark red (high density), the dotted line is the 1:1.

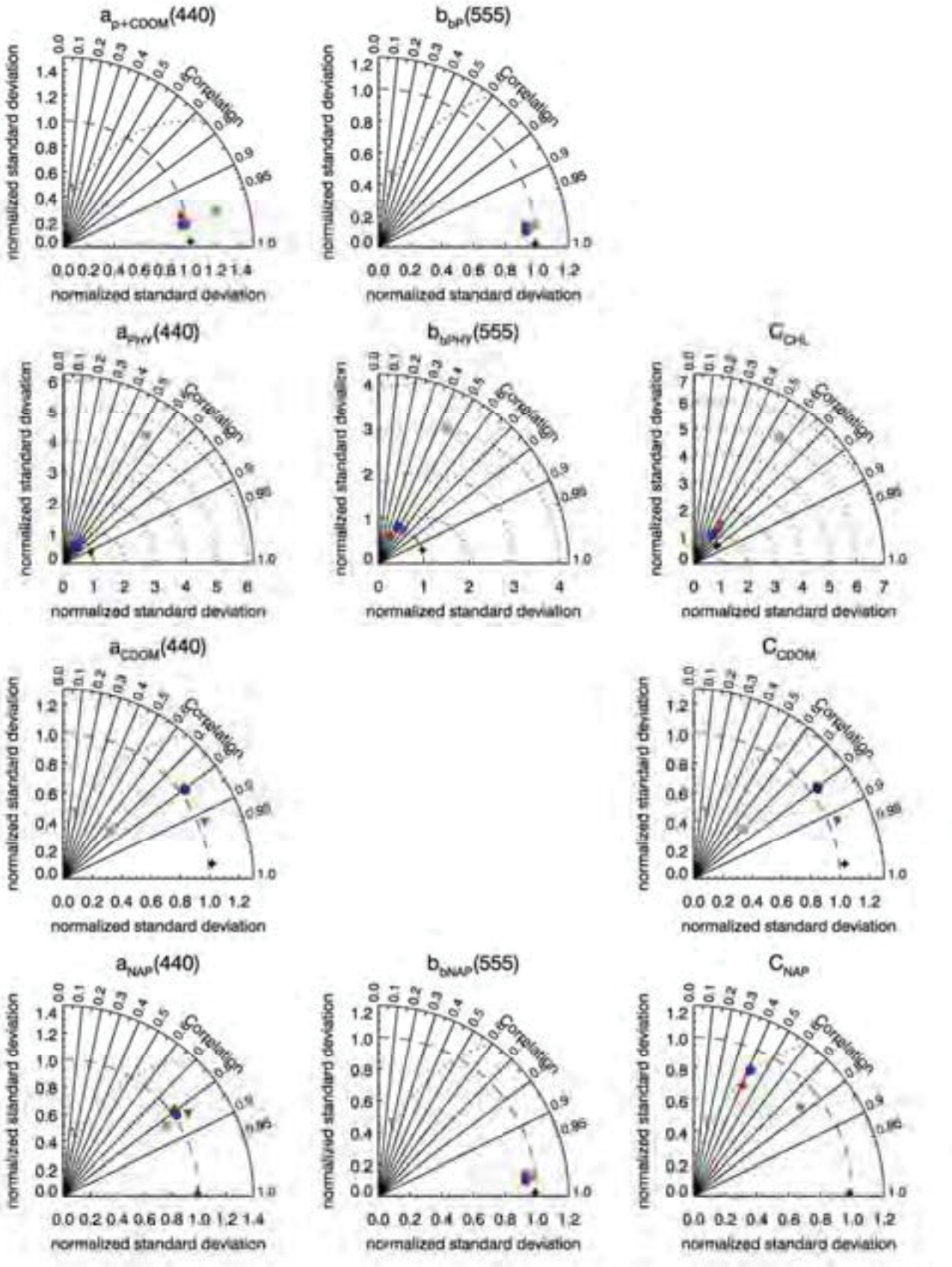

Figure 10 Accuracy of the retrieval of IOPs and concentrations: Taylor diagrams summarising the inversion performance of the four adaptive paramerizations (VDG_D, VDG_w, VDG_{DW} and VDG_S) as compared to the reference inversion (OWN_{LEE}).The figure is organized in four rows (bulk IOPs, PHY, CDOM, and NAP properties), and in three columns (a, bb, and concentrations). Symbols: Black star=OWN, green box=VDG_W, red diamond=VDG_D, blue circle=VDG_{DW}, purple triangle=VDG_S

In summary, in Figure 10 it is evident how, in this sensitivity analysis, the “complete” and the “seasonal” parameterizations (VDG_{DW} and VDG_S) lead to more accurate retrievals of the apportioned IOPs and concentrations, while the VDG_w wet season parameterization leads to the less accurate retrievals particularly for the phytoplankton-related properties (a_{PHY}, b_{bPHY} and C_{CHL}).

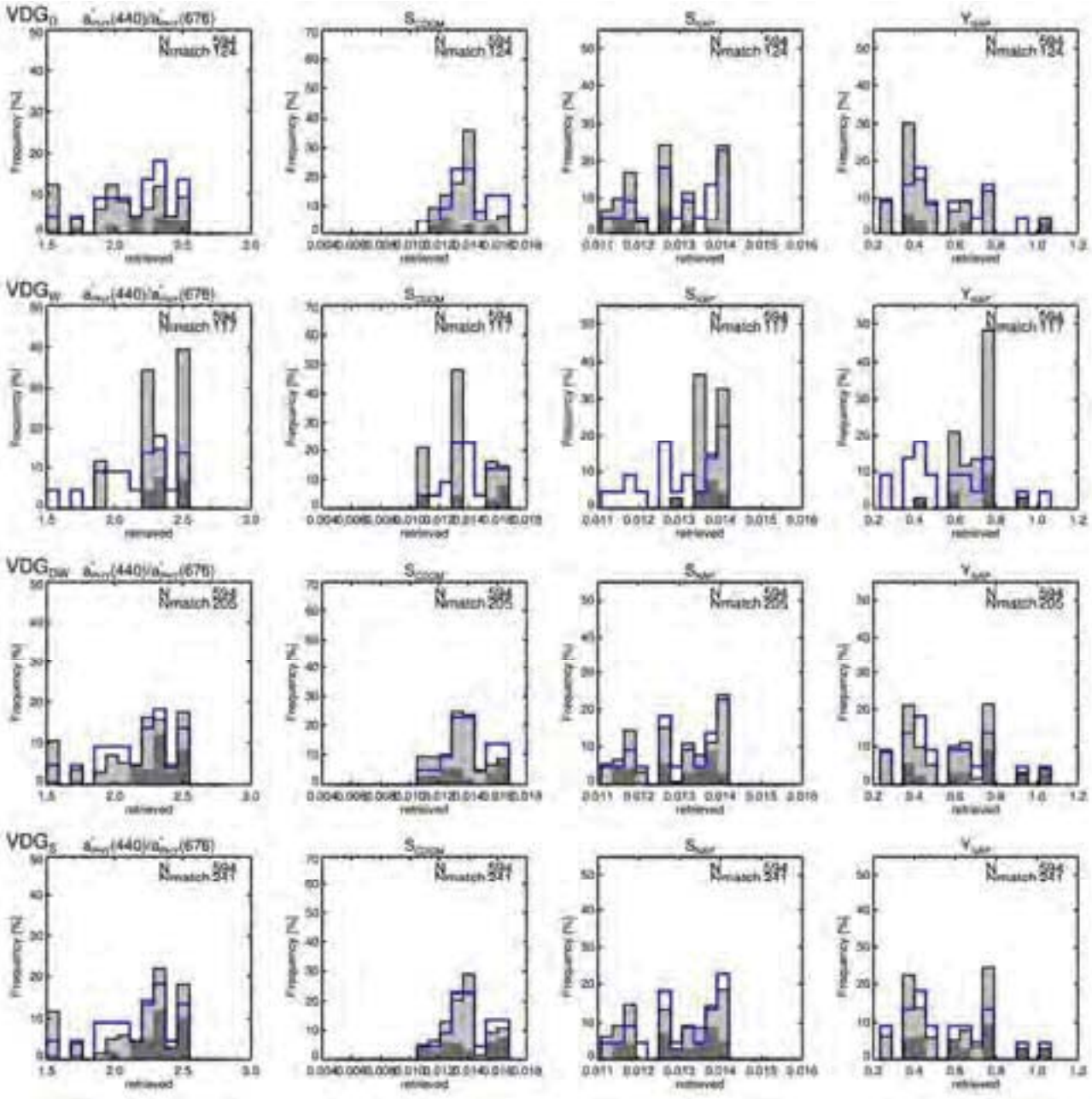

Figure 11 Distribution of accuracy of the retrieval of SIOPs shape parameters for aLMI. The figure is organized in four rows (four model parameter sets: VDG_D, VDG_w, VDG_{DW} and VDG_S), and in four columns ($a^*_{PHY}(440)/a^*_{PHY}(676)$, S_{CDOM}, S_{NAP}, and Y_{NAP}). The blue histogram presents the distribution of the SIOP parameters in the input dataset and the dark bars represent the number of solutions for which the SIOP shape and amplitude parameter set used in the forward simulation were correctly selected during the aLMI minimization process.

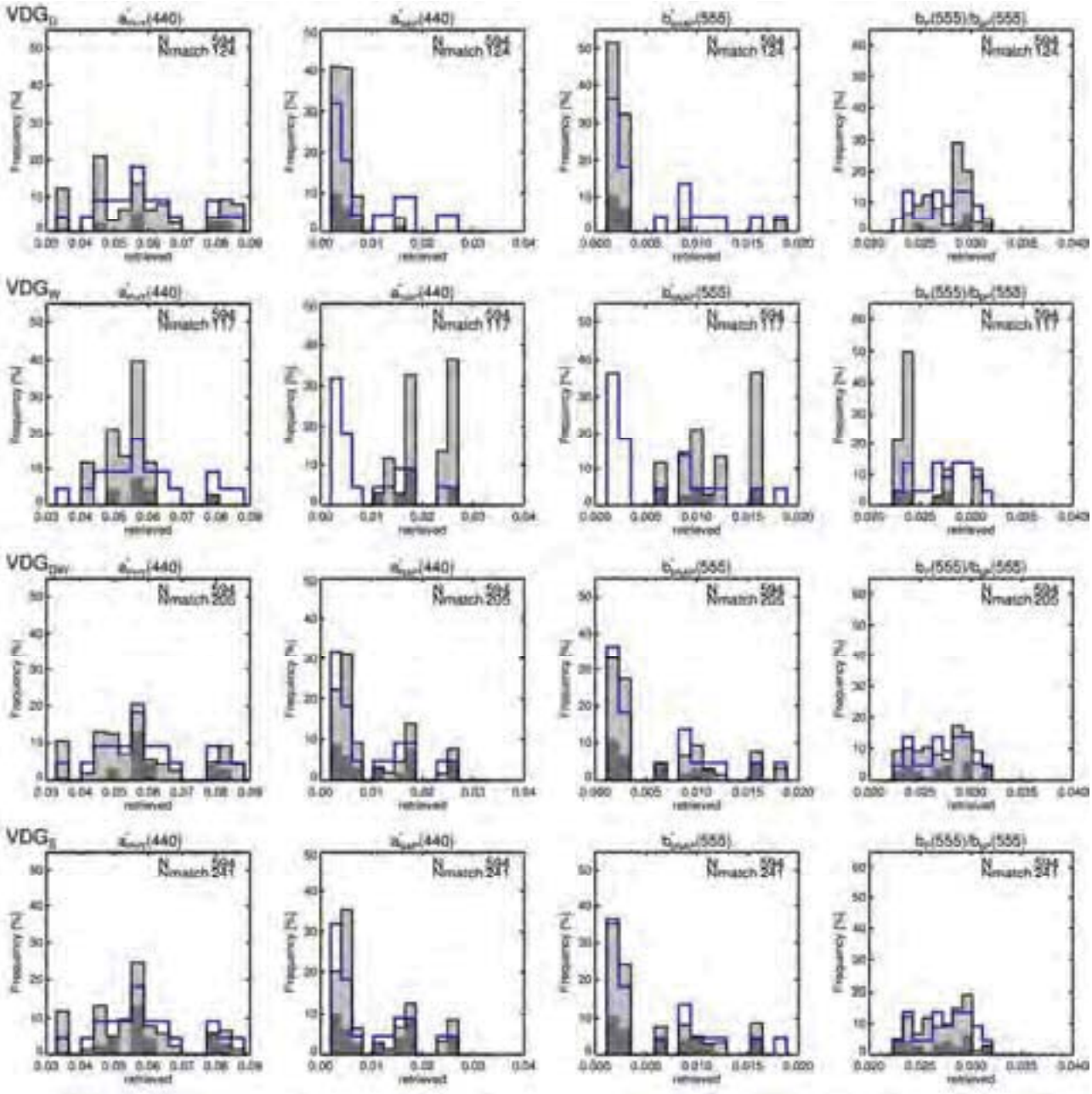

Figure 12 Distribution of accuracy of the retrieval of SIOPs amplitude parameters for aLMI. The figure is organized in four rows (four model parameter sets: VDG_D, VDG_w, VDG_{DW} and VDG_S), and in four columns ($a^*_{PHY}(440)$, a^*_{NAP}, $b^*_{b\ NAP}$, $b_{bP}(555)/b_P(555)$). The dark bars represent the number of solutions for which the SIOP shape and amplitude parameter set used in the forward simulation were correctly selected during the aLMI minimization process.

To evaluate whether the "complete" and the "seasonal" parameterizations (VDG_{DW} and VDG_S) accurately captured the seasonal variability, the aLMI inversion was performed for both parameterizations on the MODIS imagery acquired in March 2012 and in September 2013 during wet and dry season conditions. In the inversions with the "complete" parameterization (VDG_{DW}) wet season SIOP sets were erroneously selected in the dry season imagery (results not shown).

Hence for this study the MODIS inversion with "seasonal" parameterization (VDG_S) was selected as the most appropriate and was implemented for further processing of the entire MODIS water quality time series.

5 Results and discussion

This section briefly presents the validation and application of the remote sensing algorithm (based on VDG_S parameterization) to selected dry and wet season MODIS imagery to evaluate the spatial distribution of water quality products, as well as extracted time series data for selected sites to evaluate the seasonal variability of these products.

5.1 Product evaluation

The performance of the in-water retrieval algorithm was evaluated by match-up analysis (Figure 13), extracting 3x3 satellite pixels from the processed MODIS images at the location of the in-situ measurements and comparing the median with the in-situ measured water quality within a maximum time window of ±4 hours to the satellite overpasses. Match-ups were retrieved using spherical geometry by calculating the minimum distance between in-situ and satellite recorded pixel coordinates on the surface of the Earth (great circle distance). A valid match-up required the location difference to be less than 0.01 degree in both latitude and longitude dimensions. This maximum distance accuracy criterion is thus at pixel level given the one kilometre spatial resolution of the MODIS data. Flags were applied for quality control and exclusion of erroneous and out-of-range pixels. In detail, we flagged land, clouds, and high sun glint in addition to high sun angles above 75 degrees and observer zenith angles above 60 degrees using the SeaDAS provided Level 2 flags. In addition, we excluded pixels with atmospheric correction out-of-range conditions. Further, a valid match-up required at least 6 out of 9 pixels of the match-up area to be valid (unflagged).

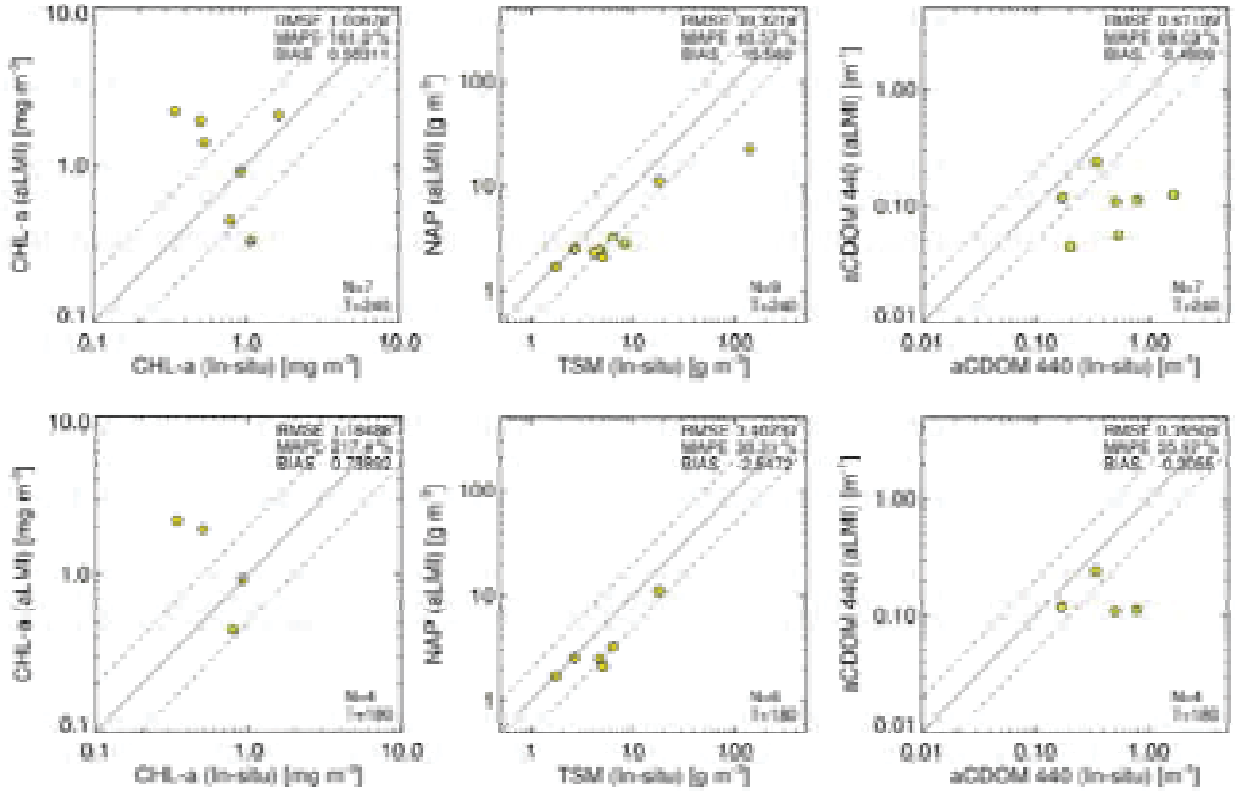

Figure 13 Results of the match-up analysis comparing satellite retrieved water quality against ground measurements of CHL, TSS or NAP and CDOM. Match-up areas are 3-by-3 pixels centred at the locations of the ground observations with a maximum time difference of ±4 hours (top) and ±3 hours (bottom panels).

The total number of observations for this match-up exercise was very limited. Applying the above criteria to all wet and dry season field observations, we only obtained 4-6 and 7-9 in-situ data points (product dependent) that can be directly compared with the satellite retrievals at ±3 and ±4 hour time differences, respectively. For coastal waters, especially those with strong tidal influence, it is generally recommended to apply much shorter time differences of up to ±30 min only (Doerffer, 2002). Statistics of Mean Absolute Percentage Error (MAPE), Root Mean Squared Error (RMSE) and bias were used to evaluate inversion performance.

Chlorophyll-a match-ups at ±4 hours revealed a MAPE of 161%, with an absolute error of RMSE 1.0 mg m^{-3} and a positive bias of 0.5 mg m^{-3} within the measured concentration range of 0.03-0.2 mg m^{-3} chlorophyll-a (Figure 13). At ±3 hours valid observations reduce to only 4 data points. This sample size is certainly insufficient to compute robust statistics; however we decided to include the ±3 hour results to evaluate the potential impact of tidal differences on the retrievals. At ±3 hours the in-situ measured concentration range reduced to 0.03-1 mg m^{-3} showing an increase of retrieval errors (MAPE=217%, RMSE=1.2 mg m^{-3} and bias=0.7 mg m^{-3}).

The percentage retrieval error for CDOM absorption at 440 nm, based on 7 samples within the measured range of 0.2-2 m^{-1} at ±4 hour time difference, was 69% with a corresponding RMSE of 0.7 m^{-1} and a negative bias of -0.5 m^{-1}. Reducing the match-up time window to ±3 hours reduced the in-situ range to 0.2-0.8 m^{-1} and resulted in a slightly improved retrieval accuracy (MAPE=56%, RMSE=0.4 m^{-1}, and bias=-0.3 m^{-1}, N=4). Also the CDOM sample size at this time step (N=4) remains insufficient to conclude on algorithm performance.

Overall best results were obtained for TSS. At ±4 hours matching-up 9 samples within the measured concentration range of 2-140 g m^{-3} resulted in a MAPE of 44%, a RMSE of 39.3 g m^{-3} and a negative bias of -15.6 g m^{-3}. Similar to CDOM, restricting the time window to ±3 hours further improved retrieval accuracy for TSS (MAPE=33%, RMSE 3.4 g m^{-3}, bias=-2.5 g m^{-3}, N=6) within the reduced in-situ concentration range of 2-20 g m^{-3}.

For the seasonally, TSS and CDOM-dominated waters of the Van Diemen Gulf, chlorophyll-a remains the most difficult water quality parameter to retrieve from remote sensing as phytoplankton only contributes ~5-20% to the total absorption budget. Retrieval errors of around 100% are realistic for this type of optically complex water and have hampered accurate retrieval in other regions of the world such as the CDOM-dominated Baltic Sea (Darecki and Stramski, 2004). Validation results from an earlier algorithm implementation for the Great Barrier Reef (see 4.2) showed chlorophyll-a errors of around 90% in less turbid waters using a more comprehensive validation data set of N=266 samples within ±3 hours (King et al., 2014). Similarly, the retrieval errors obtained for CDOM in the Van Diemen Gulf are within the expected range for optically complex waters. In comparison, the CDOM accuracy of the GBR-algorithm is 77% (N=16, ±3 hours), however for a concentration range, a magnitude lower than that found in the Van Diemen Gulf. The TSS retrieval error of ~40% obtained for the Van Diemen Gulf waters is exceptionally low compared to GBR where the TSS error is ~70% obtained from a more representative validation data set of N=114 observations within ±3 hours time difference.

In conclusion, these results should be regarded as preliminary due to the limited sample size of the Van Diemen Gulf validation data set and consequently the selected large time differences between in-situ and satellite observations. A challenge in these highly dynamic and often spatially inhomogeneous environments is the scaling problem. The satellite integrates over a larger area on the surface whereas the ground measurements represent point observations. The representativeness of such point measurements with respect to the satellite observations may be questioned in these highly dynamic waters and many more concurrent in-situ and satellite observations are needed to the evaluate algorithm performance comprehensively.

5.2 Seasonal variability

To evaluate the temporal variability of the remotely sensed water quality products, we analysed the full (11+ year) MODIS-Aqua time series and extracted 3x3 pixels from the satellite retrieved products at the

locations of the field observations (Figure 14). For illustration purpose the TSS, CHL and CDOM time series data are presented only for station VDG-D08 (Figure 2) along with number of valid pixels for each extraction (maximum 9).

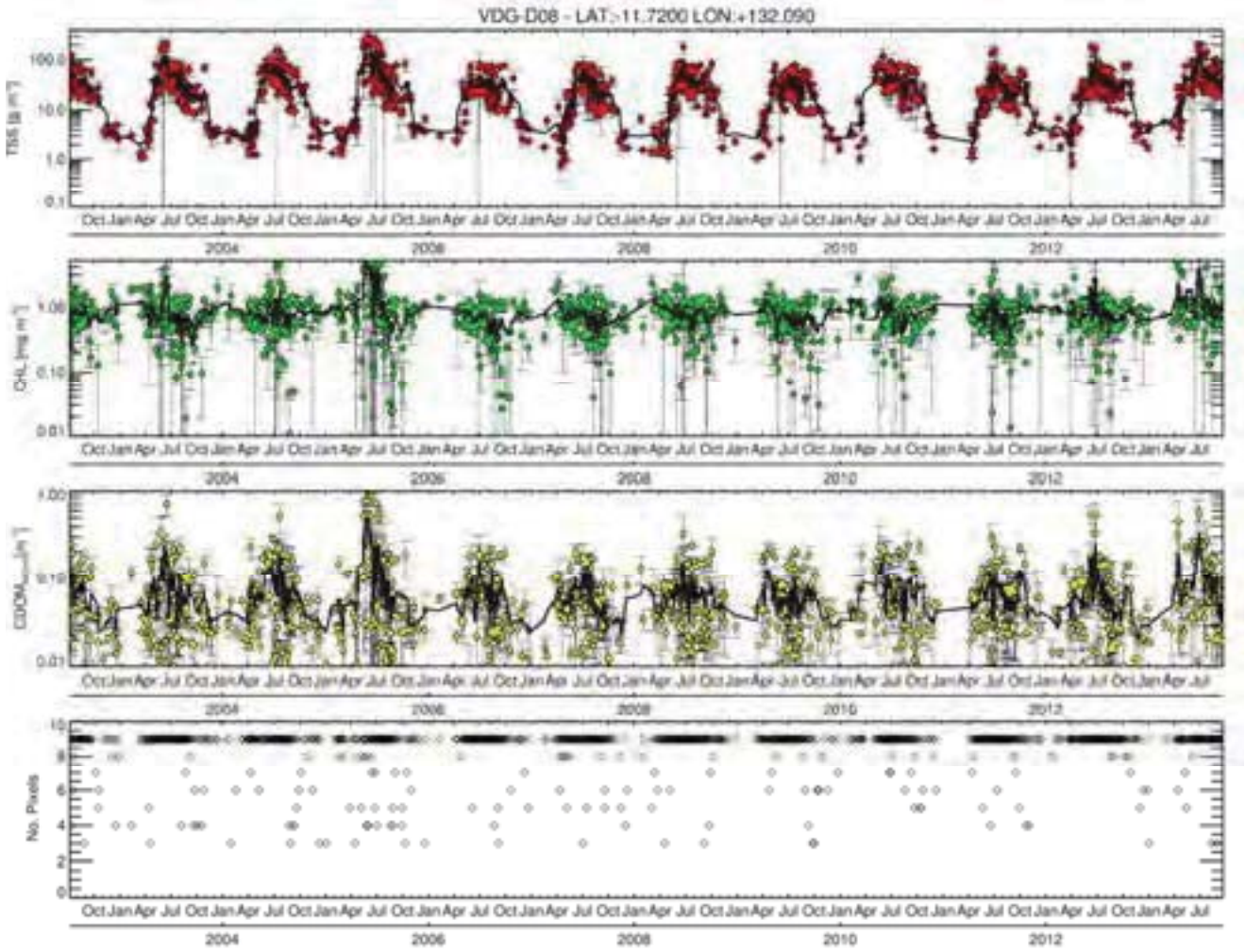

Figure 14 Temporal variability of key water quality parameters calculated from daily MODIS-Aqua imagery at station D08 to illustrate their temporal variability. Data was extracted for a 3x3 pixel box. Panels from top to bottom: Total suspended solids, Chlorophyll-a, CDOM absorption and number of valid pixels for each extraction. Solid lines represent averaged data using a 3-day window.

Large data gaps with low numbers of valid pixels can be observed during the wet season months (Nov-Apr). These are a result of cloud cover, which limits optical remote sensing from space during these months in this region; still distinct seasonal cycles in water quality parameters can be identified.

The temporal variability of TSS showed the most pronounced seasonal cycles with concentration differences ranging two orders in magnitude. Maximum TSS concentrations, in July, were consistently observed with average values ranging between 100-200 g m^{-3}, while concentration minima usually occurred in April at the end of each wet season with values around 1 g m^{-3} TSS. Lower concentrations may have occurred at times during the wet season when remote sensing observations were restricted by cloud cover. The observed seasonal variability of TSS is consistent with the findings of Blondeau-Patissier et al. (2014) who used a different satellite sensor and remote sensing method for this same region to quantify the phytoplankton bloom dynamics. Remarkable is the observed large intra-dry-seasonal variability of TSS ranging between ~10 and 200 g m^{-3}, which can be attributed to the large tidal variability. Overall higher TSS concentrations during the dry season months are likely a result of tidal-driven resuspension amplified by the prevailing south-easterly trade winds. In contrast, wet season TSS concentrations are significantly lower as river runoff into the Van Diemen Gulf is largely filtered through most of the Kakadu National Park

wetlands (20,000 km^2), possibly explaining the surprisingly low concentrations obtained from remote sensing. Higher dry and lower wet season concentrations were also confirmed by the 2012 and 2013 field observations (see BP09-fig 5A in Figure 6 and Table 1).

Less pronounced is the seasonal cycle of chlorophyll-a at station VDG-D08, which appears out-of-phase with the TSS cycle. The 3-daily averaged data is still noisy and except for the years 2005 and 2013 dry season concentrations seem on average lower compared to the wet season when it is likely that more light (less TSS) and nutrients are available. Blondeau-Patissier et al. (2014) report regional differences for the temporal variability of chlorophyll-a with only the western part of the Gulf showing increased concentrations during the wet season months. A more detailed time series analysis should be performed using a larger extraction window.

The variability of CDOM at station VDG-D08 is highly correlated with the TSS time series, showing increased absorption levels during the dry seasons with average values of 0.2 m^{-1} compared to the wet season values of around 0.03 m^{-1}. CDOM can have different spectral properties depending on its source. The source of CDOM can be determined by Excitation Emission Matrix Spectroscopy (EEMS) and initial EEMS analysis (results not shown) performed on dry season dissolved organic carbon (DOC) samples revealed that the ultra-violet spectroscopic characteristics of DOC are consistent with organic matter of relatively low molecular weight. This material may arise from pore water which has been subjected to prolonged bacterial degradation of photo-bleaching of fresh CDOM produced in the water column. Tidal resuspension of deposited sediments is the mechanism by which the transfer of pore water CDOM into the water column is enhanced during the dry season. CDOM of terrestrial origin is restricted to the near-shore waters that are influenced by river run-off during the wet seasons.

5.3 Spatial variability

Figure 15 presents the spatial variability of the remotely sensed water quality products for the contrasted wet and dry season images introduced in section 3.

The spatial distribution of NAP shows the expected gradients with generally higher concentrations found in the near-shore waters of the Van Diemen Gulf. Overall dry season NAP concentrations were found to be one order of magnitude higher compared to the wet season as a result of resuspension (note the different concentration scales). Black areas indicate masked pixels from algorithm failure or masking of clouds and sun glint as present for the Darwin Harbor region in the dry season image.

Good de-correlation between NAP and chlorophyll-a was achieved in the wet season image for the passage into the Arafura Sea ~11.5°S and 131.5°-132°E that from visual inspection of the true colour image can be identified as suspended sediment. High chlorophyll-a concentrations are constrained to the coastal regions affected by river run-off in this image. The off-shore driven plume into the Arafura Sea is mainly composed of NAP. A rather uniform distribution (no gradients) of chlorophyll-a can be observed in the dry season image. Chlorophyll-a concentrations seem to be underestimated within a narrow region around 12.1°S and 131.4°-132.2°E which requires further investigation. Good decorrelation of NAP and chlorophyll-a retrievals can also be observed for the freshwater influenced coastal waters of the Van Diemen Gulf encompassing Kakadu National Park.

Off-shore CDOM values are slightly higher in the dry season image due to resuspension as discussed in the previous paragraph, while the wet season image shows a band of increased absorption values along the Van Diemen Gulf coastline influenced by river discharge. CDOM and NAP appear uncorrelated in the Alligator Rivers Region.

In summary, quantitative image interpretation revealed that the spatial features observed in remotely sensed wet and dry season water quality products are sensible and can be attributed to physical processes. Concentration ranges are in agreement with the field observations.

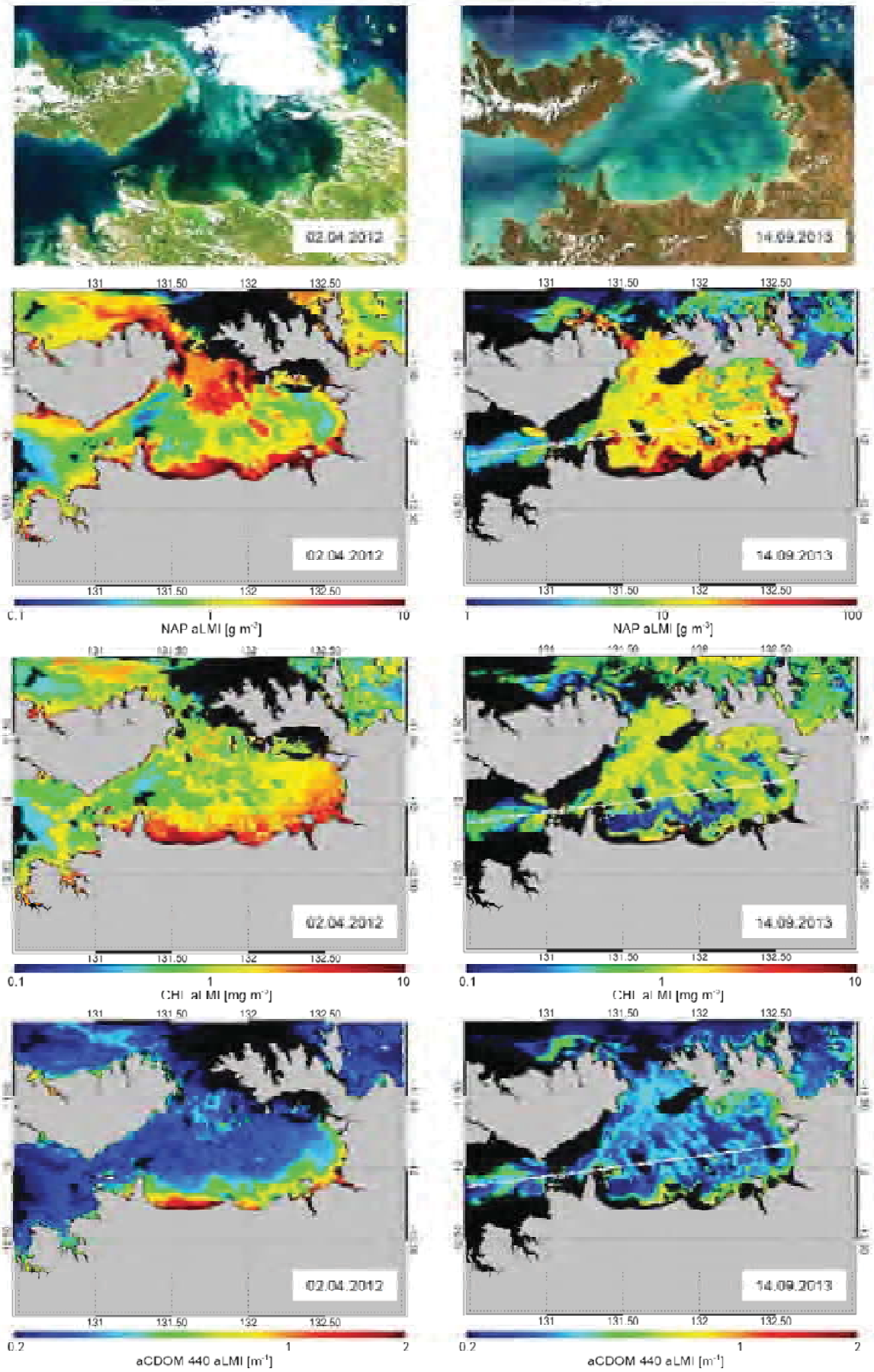

Figure 15 Spatial distribution of remotely sensed water quality during wet season (2 April 2012) and dry season (14 Sep 2013) conditions. Noted the different concentration ranges used for NAP.

6 Conclusions

This report has presented the successful development, implementation and evaluation of a physics-based inversion model to estimate water quality from MODIS-Aqua satellite observations in the Van Diemen Gulf region.

The remote sensing algorithm was parameterized with wet and dry season in-situ optical observations of the Van Diemen Gulf and was shown to have the ability to deal with the large range of optical variability typically found in this region.

In-situ optical observations revealed that the Van Diemen Gulf waters are optically complex and mainly seasonally dominated by NAP and CDOM.

A sensitivity analysis of different regional in-water algorithm parameterizations based on synthetic data showed best performance for a seasonally split algorithm implementation.

Good optical closure between in-situ measured and modelled apparent optical properties was achieved.

Product evaluation using a limited validation data set resulted in good retrieval accuracy of NAP and CDOM (44% and 69% errors respectively) for waters of this region, classified as optically complex.

Chlorophyll-a was the most difficult water quality parameter to retrieve and was associated with larger errors (160%). This is the result of phytoplankton absorption only contributing to 5-20% to the overall absorption budget.

Validation results are preliminary due to the limited number of observations and large time differences between in-situ and satellite observations in addition to the uncertainty due to the strong tidal impact in the Van Diemen Gulf region.

Remotely sensed water quality concentrations are within the range of the ground observations and observed spatial features can be attributed to physical processes such as resuspension or river run-off.

Sediment concentrations in the Van Diemen Gulf were found to be one order of magnitude higher during the dry season showing a large variability due to tidally induced resuspension – seasonal cycles of CDOM and chlorophyll-a were less pronounced.

Cloud cover limits remote sensing observations of water quality during the wet season.

7 Recommendations

Remote sensing time series data should be further analysed and linked with additional biodiversity data to detect and help explain potential trends, e.g. changes in mangrove or seagrass extents.

Remotely sensed CDOM and sediment concentrations should be used as data assimilation inputs to inform hydrodynamic and sediment transport models developed for this region.

This remote sensing approach should be adapted to geostationary satellite observations of the recently launched Himawari-8 mission operated by the Japanese Aerospace Exploration Agency (JAXA) that offers the potential to resolve tidal cycles by providing remote sensing imagery every 10 min at 1 km spatial resolution.

Regular high-quality bio-optical, geochemical and radiometric measurements should be integrated into a marine monitoring program needed for continuous support of remote sensing algorithm development and validation and integrated coastal zone management.

Management options for maintaining biodiversity of Kakadu National Park should include strategies beyond the coastal boundary of the Park as catchments and adjacent coastal marine environments are highly connected.

Acknowledgements

Funding for this study was provided by the Australian Government's National Environmental Research Program (NERP) and the CSIRO. In the final stages of this project Dr Vittorio Brando was supported by the European Union (FP7-People Co-funding of Regional, National and International Programmes, GA n. 600407) and the CNR RITMARE Flagship Project. We kindly acknowledge the support by the Australian Institute of Marine Science (AIMS) who provided ship-time on the RV Solander to conduct the wet season field voyage in collaboration the Charles Darwin University. Special thanks to Jaana Dielenberg, Amy Kimber and Michael Lawrence-Taylor for providing excellent project support and public outreach. We are grateful to our colleagues Dr Phillip Ford for conducting the EEMS analysis and Dr Yi Qin and Dr Tim Malthus for conducting internal review of this report. We also wish to thank Ms Heidi Franklin for her technical support in preparation of the fieldworks. We acknowledge the MODIS mission scientists and associated NASA personnel for the production of data used in this research effort.

Appendix A Data format description & repository

The provided water quality outputs associated with this project were stored in Hierarchical Data Format (HDF). Each of the 6,057 provided HDF files and contains the following 445x550 pixel sized data arrays of listed below.

Data pixels may become invalid due to algorithm failure or to the presence of atmospheric or oceanic conditions that cannot be corrected for, e.g. contamination due to severe sun glint or simply clouds. Quality control is essential prior to data analysis and several masks have been pre-applied to reject invalid pixels. For the purpose of this study we rejected pixels over land, high sun glint in addition to pixels affected by clouds, stray-light as well as out-of-range conditions for sun and observing geometries. A detailed overview of all SeaDAS provided masks is provided at http://oceancolour.gsfc.nasa.gov/VALIDATION/flags.html. Two additional bit masks are provided for the CSIRO ANN atmospheric correction algorithm and should be analysed in conjunction with the SeaDAS provided flags. The first ANN bit captures out-of-range conditions for all neural network inputs while the second bit provides quality control of all reflectance outputs.

Freely available and platform-independent tools such as HDFView (http://www.hdfgroup.org) can be used for visualizing and browsing of the data.

Variable	Description	Data type	Units	Valid range
longitude	Longitude	32 bit float	Degree	-180.0, 180.0
latitude	Latitude	32 bit float	Degree	-90.0, 90.0
l2_flags	Level 2 processing flags SeaDAS	32 bit integer	Dim-less	n/a
nn_flags	ANN failure flags	32 bit integer	Dim-less	n/a
Chl_MIM	Concentration of chlorophyll-a	32 bit float	$\mu g\ L^{-1}$	n/a
Nap_MIM	Concentration of non-algal particles	32 bit float	$mg\ L^{-1}$	n/a
a_phy_MIM_441	Absorption of phytoplankton 441 nm	32 bit float	m^{-1}	n/a
a_CDOM_MIM_441	Absorption of CDOM 441 nm	32 bit float	m^{-1}	n/a
a_tot_MIM_441	Total absorption 441 nm	32 bit float	m^{-1}	n/a
bb_phy_MIM_551	Back-scattering of phytoplankton 551 nm	32 bit float	m^{-1}	n/a
bb_P_MIM_551	Back-scattering of particles 551 nm	32 bit float	m^{-1}	n/a
bb_NAP_MIM_551	Back-scattering of non-algal particles 551 nm	32 bit float	m^{-1}	n/a

A copy of the MODIS water quality time series can be obtained from the CSIRO Data Access Portal at:

http://dx.doi.org/10.4225/08/550B4DD2162D1

Appendix B Symbols and abbreviations

Symbol/abbreviation	Description	Units
CHL	Chlorophyll-a	mg m^{-3}
NAP	Non-algal particles	g m^{-3}
TSS	Total suspended solids	g m^{-3}
Y_{NAP}	Power law exponent for the NAP backscattering coefficient	–
S_{NAP}, S_{CDOM}	Spectral slope of NAP or CDOM	nm^{-1}
a	Total absorption coefficient	m^{-1}
a_{PHY}, a_{PHY}*	Absorption, and specific absorption coefficient by phytoplankton	m^{-1}
a_{CDOM}	Absorption coefficient by CDOM	m^{-1}
a_{NAP}, a_{NAP}*	Absorption and specific coefficient by NAP	m^{-1}
b_b	Total backscattering coefficient	m^{-1}
c	Attenuation coefficient	m^{-1}
R_{rs}, r_{rs}	Above and below water remote sensing reflectance	sr^{-1}
λ	Wavelength	nm
aLMI	Adaptive Linear Matrix Inversion	
ANN	Artificial Neural Network	
AOP	Apparent Optical Property	
CDOM	Coloured Dissolved Organic Matter	
DOC	Dissolved Organic Carbon	
EEMS	Excitation Emission Matrix Spectroscopy	
GBR	Great Barrier Reef	
FOV	Field of view	
SeaDAS	SeaWiFS Data Analysis System	
IOP	Inherent Optical Property	
IMOS	Integrated Marine Observing System	
JAXA	Japanese Aerospace Exploration Agency	

MAPE	Mean Absolute Percentage Error
MODIS	Moderate Resolution Imaging Spectrometer
NASA	National Aeronautic and Space Administration
NCI	National Computational Infrastructure
NERP	National Environmental Research Program
NOAA	National Oceanic and Atmospheric Administration
SIOP	Specific Inherent Optical Property
Stdev	Standard deviation
RMSE	Root Mean Squared Error
TOA	Top of Atmosphere
VDG	Van Diemen Gulf

References

Brando, V. E. and A. G. Dekker (2003), Satellite hyperspectral remote sensing for estimating estuarine and coastal water quality. IEEE Trans.Geosci.Remote Sens. 41(6): 1378-1387.

Brando, V. E., A. G. Dekker, T. Schroeder, Y. J. Park, L. A. Clementson, A. Steven and D. Blondeau-Patissier (2008), Satellite retrieval of chlorophyll CDOM and NAP in optically complex waters using a semi-analytical inversion based on specific inherent optical properties. A case study for Great Barrier Reef coastal waters. Ocean Optics XIX, Barga, Italy.

Brando, V. E., A. G. Dekker, Y. J. Park, and T. Schroeder (2012), An adaptive semi-analytical inversion of ocean colour radiometry in optically complex waters, *Applied Optics*, *51*(15), 2808-2833.

Brando V.E., Schroeder T., King E., and Dyce P. (2014), Reef Rescue Marine Monitoring Program: Using Remote Sensing for GBR-wide water quality, Final Report for 2013/14 Activities, CSIRO Report to the Great Barrier Reef Marine Park Authority, 217 pp.

Blondeau-Patissier, D., V. E. Brando, K. Oubelkheir, A. G. Dekker, L. A. Clementson and P. Daniel (2009), "Bio-optical variability of the absorption and scattering properties of the Queensland inshore and reef waters, Australia." J. Geophys. Res. 114.

Blondeau-Patissier, D., T. Schroeder, V. E. Brando, S. W. Maier, A. G. Dekker, and S. Phinn (2014), ESA-MERIS 10-Year Mission Reveals Contrasting Phytoplankton Bloom Dynamics in Two Tropical Regions of Northern Australia, *Remote Sens.*, *6*(4), 2963-2988.

Boss, E., W. S. Pegau, M. Lee, M. Twardowski, E. Shybanov, G. Korotaev, and F. Baratange (2004), Particulate backscattering ratio at LEO 15 and its use to study particle composition and distribution, *Journal of Geophysical Research*, *109*(C1), C01014.

Chang G.C., Dickey T.D., Mobley C.D., Boss E., Pegau W.S. (2003), Toward optical closure of upwelling radiance in coastal waters, Applied Optics, 42(9), 1574-1582.

Clementson, L.A. (2013), The CSIRO method *in* Hooker, S.B., L. Clementson, C.S. Thomas, L. Schlüter, M. Allerup, J. Ras, H. Claustre, C. Normandeau, J. Cullen, M. Kienast, W. Kozlowski, M. Vernet, S. Chakraborty, S. Lohrenz, M. Tuel, D. Redalje, P. Cartaxana, C.R. Mendes, V. Brotas, S.G. Prabhu Matondkar, S.G. Parab, A. Neeley, and E. Skarstad Egeland , 2013. The Fifth SeaWiFS HPLC Analysis Round-Robin Experiment (SeaHARRE-5). NASA Technical Memorandum 2012-217503, NASA Goddard Space Flight Center, Greenbelt, Maryland.

Darecki, M., and D. Stramski (2004), An evaluation of MODIS and SeaWiFS bio-optical algorithms in the Baltic Sea, *Remote Sensing of Environment*, *89*(3), 326-350.

Doerffer, R. (2002), Protocols for the validation of MERIS water products. European Space Agency Doc. No. PO-TN-MEL-GS-0043.

Fu G., Baith K.S., and McClain C.R. (1998), SeaDAS: The SeaWiFS Data Analysis System, in *Proceedings of the 4th Pacific Ocean Remote Sensing Conference*, Qingdao, China.

Giardino, C., V. E. Brando, A. G. Dekker, N. Strömbeck and G. Candiani (2007). "Assessment of water quality in Lake Garda (Italy) using Hyperion." Remote Sensing of Environment 109(2): 183-195.

Gordon, H. R., Brown, O. B., Evans, R., Brown, J., Smith, R. C., Baker, K. S., and Clark, D. C. (1988), A semianalytical model of ocean colour, J. Geophys. Res. 93, 10909–10924.

Goyens, C., Jamet C., and Schroeder, T. (2013), Evaluation of four atmospheric correction algorithms for MODIS-Aqua over contrasted coastal waters, Remote Sens. of Environ., 131, 63-75.

Hoge, F. E. and Lyon, P. E. (1996), Satellite retrieval of inherent optical properties by linear matrix inversion of oceanic radiance models—an analysis of model and radiance measurement errors, J. Geophys. Res. 101, 16631–16648.

IOCCG (2010), Atmospheric Correction for Remotely-Sensed Ocean-Colour Products, Wang, M. (ed.), Reports of the International Ocean-Colour Coordinating Group, No. 10, IOCCG, Dartmouth, Canada.

Jolliff, J.K., Kindle, J.C., Shulman, I., Penta, B., Friedrichs, M.A.M., Helber, R., Arnone, R.A. (2009), Summary diagrams for coupled hydrodynamic-ecosystem model skill assessment. J. Mar. Syst. 76, 64–82.

Kennedy, K., Schroeder, T., Shaw, M., Haynes, D., Lewis, S., Bentley, C., Paxman, C., Carter, S., Brando, V., Bartkow, M., Hearn, L., Mueller, J. (2012) Long term monitoring of photosystem II herbicides – Correlation with remotely sensed freshwater extent to monitor changes in the quality of water entering the Great Barrier Reef, Australia. Marine Pollution Bulletin 65, 292–305.

King E. A., Schroeder T., Brando V. E., Suber K. (2014), A pre-operational System for Satellite Monitoring of the Great Barrier Reef Marine Water Quality, CSIRO Wealth from Oceans Flagship report.

Lee, Z., Arnone, R., Hu, C., Werdell, P. J., and Lubac, B. (2010), Uncertainties of optical parameters and their propagations in an analytical ocean color inversion algorithm, Appl. Opt. 49, 369–381.

Lyon, P. and Hoge, F. (2006), The Linear Matrix Inversion Algorithm, in IOCCG Report Number 5, Remote Sensing of Inherent Optical Properties: Fundamentals, Tests of Algorithms, and Applications, Z. Lee, ed. (IOCCG, 2006), pp. 49–56.

Oubelkheir, K., Ford P.W., Clementson L.A., Cherukuru N., Fry G. and Steven A.D.L. (2014), Impact of an extreme flood event on optical and biogeochemical properties in a sub-tropical coastal peri-urban embayment (Eastern Australia). J. Geophys. Res. (Oceans), 119(9), 6024-6045.

Schroeder, T., Behnert, I., Schaale, M., Fischer, J., and Doerffer, R. (2007), Atmospheric correction algorithm for MERIS above case-2 water, International Journal of Remote Sensing **28**, 7, 1469-1486.

Schroeder, T., M. J. Devlin, V. E. Brando, A. G. Dekker, J. E. Brodie, L. A. Clementson, and L. McKinna (2012), Inter-annual variability of wet season freshwater plume extent into the Great Barrier Reef lagoon based on satellite coastal ocean colour observations, *Marine Pollution Bulletin*(65), 210-233.

Taylor, K. E. (2001), Summarizing multiple aspects of model performance in a single diagram, J. Geophys. Res., 106, D7, 7183-7192.

Tilstone, G.H., Moore, G.F., Sorensen, K., Doerffer, R., Rottgers, R., Ruddick, K., Pasterkamp, R. (2002). REVAMP protocols: regional validation of MERIS chlorophyll products in North Sea coastal waters. European Space Agency.

Xiong, X., and W. Barnes (2006), An Overview of MODIS Radiometric Calibration and Characterization, *Advances in Atmospheric Sciences*, *23*, 69–79.

CONTACT US

t 1300 363 400
+61 3 9545 2176
e enquiries@csiro.au
w www.csiro.au

YOUR CSIRO

Australia is founding its future on science and innovation. Its national science agency, CSIRO, is a powerhouse of ideas, technologies and skills for building prosperity, growth, health and sustainability. It serves governments, industries, business and communities across the nation.

FOR FURTHER INFORMATION

Oceans & Atmosphere Flagship
Dr Thomas Schroeder
t +61 7 3833 5581
e Thomas.Schroeder@csiro.au